NUMERICAL STUDY OF DROP FORMATION FROM DRIPPING TO JETTING

by

ALLOUAH KADJO

Presented to the Faculty of the Graduate School of
The University of Texas at Arlington in Partial Fulfillment
of the Requirements
for the Degree of

MASTER OF SCIENCE IN MECHANICAL ENGINEERING

THE UNIVERSITY OF TEXAS AT ARLINGTON
DECEMBER 2011

ACKNOWLEDGEMENTS

I would like to express my deepest appreciation and gratitude to my advisor Dr. Albert Tong for his guidance, support and encouragement throughout my research. I am really thankful for his time and patience during our meetings.

I would also like to thank my committee members Dr. Dereje Agonafer and Dr. Ratan Kumar. I want to acknowledge my group members for their help, advices and friendship.

I am grateful to my family for their patience, support and understanding.

May 18, 2011

ABSTRACT

NUMERICAL STUDY OF DROP FORMATION

FROM DRIPPING TO JETTING

Allouah Kadjo, M.S.

The University of Texas at Arlington, 2011

Supervising Professor: Albert Y. Tong

The formation of liquid droplet from a capillary tube has been examined using numerical simulations. The dimensions of the capillary tube and the flow velocity have been varied to observe the regimes of drop formation. There are three main regimes of drop formation, which are the periodic dripping, the dripping faucet and the jetting regimes. The mechanism of drop formation changes from one regime to another and involves different parameters. A particular emphasis has been placed on the velocity limits between the different regimes and the critical role played by instabilities in the generation of satellite drops. The algorithm used for modeling the free surface of the fluid is the Coupled Level Set Volume of Fluid (CLSVOF) scheme, which incorporates both the Volume of Fluid (VOF) method for tracking and locating the free surface, and the Level Set (LS) method for the estimation of the local curvature. The free surface is reconstructed by the Piecewise Linear Interface Calculation (PLIC) scheme and the surface force is estimated by the Continuum Surface Force (CSF) model. The accuracy of the numerical study has been validated by the comparison to empirical data available in the literature.

TABLE OF CONTENTS

LIST OF ILLUSTRATIONS

,

LIST OF TABLES

CHAPTER 1

INTRODUCTION

1.1 Problem Statement

The phenomenon of drop formation from a nozzle is very complex and has been extensively studied for more than a century. It has applications in multiple domains like ink-jet technologies, spray painting, distillation and mixing processes. In fact, the formation of drop is very important in those domains because there is a need to obtain liquid drops of precise sizes. Understanding the different factors participating in the breakup of the pendant drop is of major importance since it will allow control of those parameters to attain the desired goals.

There are three main regimes of drop formation from a capillary tube. In order to observe the different regimes, the velocity of the fluid at the tube inlet is increased until the different limits between the regimes are reached. For low flow rates, there is the periodic dripping regime where the drops are formed at regular time interval and have roughly the same size. When the flow rate is slightly increased, the successive drops have different sizes but are still formed periodically; this regime of drop formation is the dripping faucet. With further increase of the flow rate, the dripping faucet gives way to the jetting where the detachment point of the drops moves away from the tube exit until eventually the drops are formed from the end of a long liquid column. The dynamics of drop formation differ from one regime to another and involve a competition between the inertial, capillary, surface tension, gravitational forces and the growth of instabilities.

The objective of this study is to examine the mechanism of drop creation from dripping to jetting and to determine the velocity limits between the different regimes. The subject of liquid droplet formation has been investigated experimentally, theoretically and numerically over the years. Most researches study the breakup mechanism in either the dripping or jetting mode, but

few have covered in great details the full range of drop formation from dripping to jetting, and even fewer have acknowledged the chaotic behavior during the transition from dripping to jetting. Experimental investigations of the different regimes are difficult. Because the space scale and the pinch off time are very small, very sophisticated devices are needed for accurate studies. Numerical studies are also challenging because this is a moving boundary problem with surface tension on the free surfaces; and modeling this type of flow is quite hard due to discontinuity issues. Moreover the singularity that occurs at the moment of breakup of the drop increases the degree of complexity.

The present study is a numerical simulation which uses a version of RIPPLE which has been modified by a researcher group at the University of Texas at Arlington under the supervision of Professor Albert Y. Tong. RIPPLE is a computational fluid dynamic tool for modeling transient, two-dimensional, incompressible fluid flows with surface tension on free surfaces. RIPPLE was originally developed at Los Alamos National Laboratory and uses the Volume of Fluid (VOF) scheme to determine the free surface [1]. The VOF scheme has very good mass conservation properties but lacks accuracy on the normal and curvature calculations. Since many problems in the domain of fluid dynamics involve large local curvature, some modifications were made and the Level Set (LS) method which accurately computes the interface normal vector and shapes was added. The new algorithm used for the free surface tracking is a combination of the VOF and LS methods and is called the Coupled Level Set Volume of Fluid (CLSVOF) method. Once the free surface has been computed using the CLSVOF method, it is reconstructed via a Piecewise Linear Interface Construction (PLIC) scheme. In order to calculate the surface tension force present on the free surface, the Continuum Surface Force (CSF) model is used.

To validate the numerical results, comparisons with experimental data [2] have been made and a fair agreement was found.

1.2 Organization of Thesis

In Chapter 2, an overview of the different regimes of drop formation is given, along with a literature review of the different studies which have been done on the subject. The numerical scheme used for the simulation is presented in Chapter 3. In Chapter 4, the results of the numerical simulations are compared to some empirical data and the mechanisms of drop formation are explained in detail. Chapter 5 concludes the study and states the future work.

CHAPTER 2

OVERVIEW OF THE REGIMES OF DROP FORMATION

2.1 Introduction

A number of researchers have conducted experimental and numerical studies on the formation of drops from a vertical tube. There are three main regimes of drop formation, which are the periodic dripping, the dripping faucet and the jetting. The periodic dripping and dripping faucet are both periodic regimes with the only difference being that in the periodic dripping regime the drops have the same size where in the dripping faucet regime the drop sizes vary. In the jetting regime, the drops detach from the ends of long liquid columns. Clanet and Lasheras [2] studied the three regimes and found experimentally and theoretically the critical Weber number at which the transition from the periodic regimes to jetting occurs. The investigation was done using tubes of different diameters and gradually increasing the inlet velocity until the limits between the different regimes were reached. The experimental results obtained by Clanet and Lasheras [2] are used for comparison in the present numerical study.

As mentioned previously, in the periodic dripping regime, the drops are formed at regular time interval and have roughly the same size; those characteristics are desirable in multiple industries where it is important to produce drops of uniform size. Many studies have been reported on the periodic dripping regime and particularly on the volume of the drops. Tate [3], one of the first researchers in the domain of drop formation, calculated the mass of the pendant drop by equating the surface tension and gravitational forces. There are also the studies by Rayleigh [4] who conducted a dimensional analysis and used a correction factor determined experimentally for a better approximation of the mass of the drop. The correction factor, refined many years later by Harkins and Brown [5], is quite accurate and is one of the methods currently used to calculate the surface tension. Other studies on the periodic dripping

mode showed the importance of the fluid properties and the dimensions of the nozzle on the dynamics of drop formation. Zhang and Basaran [6] found that at low flow rates or in the dripping region, the drop is formed under the action of its weight. In part of the study, they kept the outer diameter of the nozzle and the mass flow rate constant while changing the inner diameter to study the effect of the wall thickness. As the inner tube diameter decreases, the velocity of the incoming fluid increases. Another key point in the investigation was the effect of physical properties of the fluid on the process. The conclusions of their researches were that the viscosity tends to damp the perturbations and stabilizes the growing drop, but has little effect on its volume. Also the viscosity delays the break off time of the drop, since for highly viscous fluids, the neck gets really long; increasing the time it takes for the drop to detach. The surface tension influences the volume, shape and time of the break up. By increasing the surface tension, spherical drops with bigger volume are obtained. Surface tension force increases the cohesion between the fluid elements at the surface of the drop and competes against the gravitational force for the equilibrium of the system. Therefore the greater the surface tension, the more fluid comes into the drop, and a bigger drop is formed.

In the periodic dripping regime, it was observed that for a range of Weber number, there is the formation of satellite drops after the breakup of the main drop. In some applications, the satellite drops are not desirable, so knowing the range at which there is formation of satellite drops is very important. The satellite drop is very small comparing to the primary drop and its mode of formation differs from that of the primary drop. Notz et al. [7] described in great detail the shape of the satellite drop by conducting experiments using ultrahigh speed digital imaging system. The authors [7] followed the complex shape and evolution of the liquid thread connecting the main drop to the liquid source and how it decomposes in satellite drop under the effect of capillary waves. Henderson and co-workers [8] did another study and showed that the liquid ligament could break near its end or at interior points. As the primary drop falls, the liquid ligament grows longer and thinner until it is completely detached from both the drop and the

portion of the liquid still attached to the nozzle, and forms an isolated entity. After the breakup, the unbalanced surface tension forces provoke some perturbations in the form of ripples on the surface of the ligament. The oscillations grow in magnitude creating secondary necking and bifurcation. The position of the secondary breakup depends on the most unstable wave for if the wavelength of the most unstable wave is shorter than the length of the ligament, it breaks up at interior points; otherwise, it pinches off near its ends. The type of instability that affects the ligament is the same that disturbs the uniform liquid jet, case studied by Rayleigh [9].

One of the domains of drop formation which so far has been insufficiently exploited is the dripping faucet regime or the erratic transition between periodic dripping and jetting. The publication by Subramani et al. [10] was one of the few which has done an extensive investigation of this dripping faucet regime and explained the mechanism of drop formation in that regime. They examined the dynamics of drop formation from a capillary tube, from a low to a high flow rate, by a combination of numerical computations and experiments. For their numerical studies, the one-dimensional slender-jet approximation of the 2D Navier-Stokes equation was solved by finite element analysis. It was found that the physical properties of the fluid influence the span of the dripping faucet region. For some particular cases, the dripping faucet disappeared and the system went directly from periodic to jetting. Details of those particular cases are given in Chapter 4.

There are many researchers who played a major role in explaining the phenomenon of the formation of drop from a continuous stream. Savart [11] showed that the breakup of a jet was not controlled by gravity or the type of fluid but was mostly due to the growth of undulations present on the surface of the liquid column. Later, Plateau [12] tied the surface tension to the evolution of the undulations, demonstrating the role of the surface tension in the decomposition of a liquid jet. He also discovered by empirical analysis that a jet of water, falling vertically will decompose in droplets when its length is greater than about 3.13 times its diameter. Rayleigh

[9] validated the findings of Plateau and was able to prove theoretically that there is an optimal wavelength at which waves grow fastest and which determines the size of the drop.

Empirical researches about the process of drop formation have been extensively performed; however the experimental set up, the time and length scale make numerical studies a good alternative for investigating and understanding this complex process. In numerical studies, the Navier-Stokes and continuity equations are solved with application of the boundary conditions. Basaran et al. [13] used a one-dimensional analysis through the slender-jet approximation to simplify the 2D Navier-Stokes equation. Their results were in good agreement with the experimental data. Their method had the benefit to be less computational time consuming than most numerical tools. Some numerical researches were done by Zhang [14], using RIPPLE to simulate the mechanism of drop formation and study the effect of inertial, viscous and gravitational forces. His findings were in agreement with the experiment results.

Much research has been done on the topic of drop formation from a capillary tube; some of those studies focused on the pendant drop in the periodic dripping regime while others emphasized on the creation of drop from a continuous long jet. To date, very few have covered the full range of drop formation from dripping to jetting. In the present study, the three regimes of drop formation are examined in detail and the mechanism of drop formation in each regime is explained.

2.2 Regimes of Drop Formation

There are three regimes of drop formation (Figure 2.1) which are mainly determined by the position of the detachment of the drop, the periodicity of drop formation and the drop size.

The first regime has the lowest velocity and is called periodic dripping (Figure 2.2). In this regime, the drop is formed by the gradual injection of fluid through the nozzle and is in a state of quasi-equilibrium. The drop is subject to different forces which are surface tension, gravitational, capillary and inertial forces. At a certain point, the equilibrium is broken and the drop starts accelerating and detaches from the main region. There is also the formation of a

neck or a liquid ligament. As the primary drop separates from the nozzle, the length of the neck increases while its width shrinks. After the detachment of the main drop, the ligament recoils and moves upward. For small Weber numbers or low velocities, the neck is very thin and breaks up into tiny drops called satellite drops. The satellite drops are formed due the growth of instabilities [8]. In fact, after the pinch off of the main drop, there is a generation of waves along the surface of the ligament. Those waves grow in magnitude and cause instability. The phenomenon of wave growth which helps the formation of satellite drops is similar to the Plateau Raleigh instability [9].

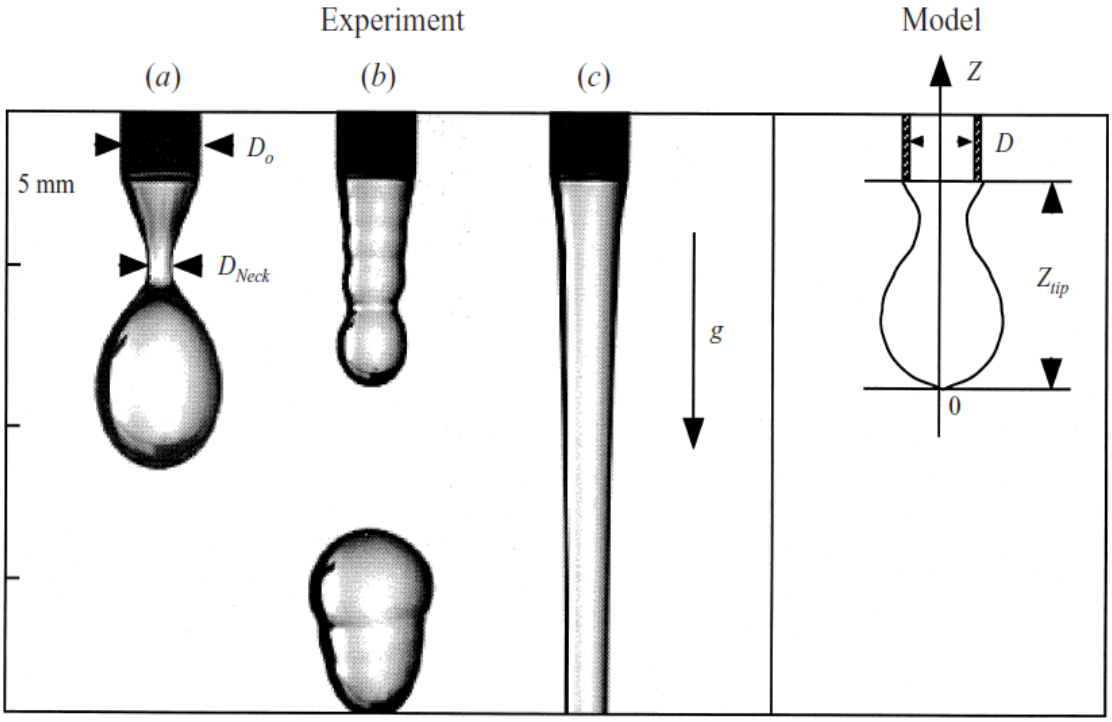

Figure 2.1 Different regimes of drop formation for a tube of inner diameter D=2.159mm and outer diameter Do=2.769mm: (a) Periodic dripping (We=0.063), (b) Dripping faucet (We=1.73), (c) Jetting (We=2.3), (We is the Weber number). [2]

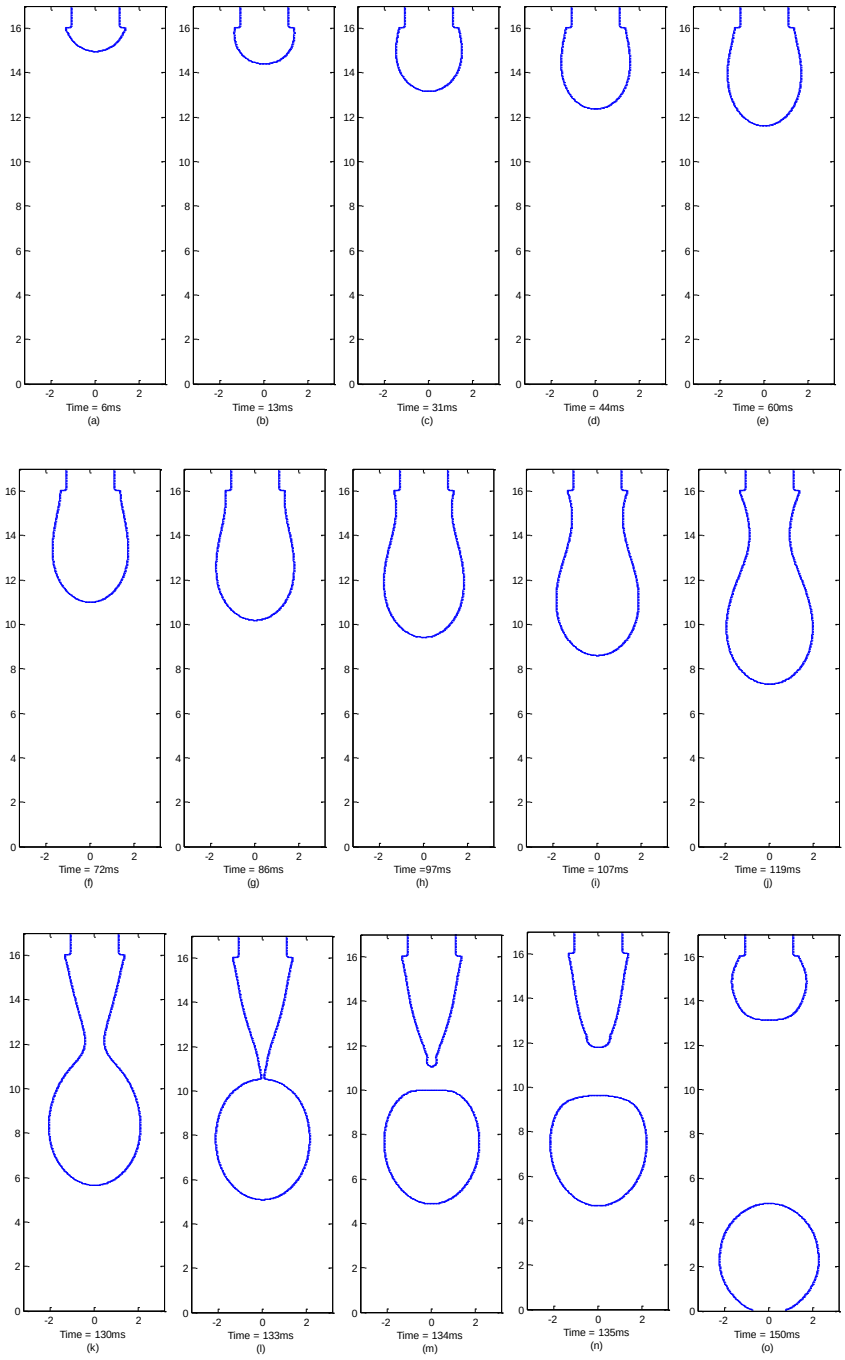

Figure 2.2 Evolution of a pendant drop from a capillary tube of inner diameter D=2.1mm and outer diameter Do=2.7mm for a liquid velocity of 0.15m/s (periodic dripping mode).

In the periodic dripping regime, there is not always formation of satellite drops after the detachment of the primary drop. As the inlet velocity of the fluid in the nozzle increases, more fluid comes into the bridge connecting the pendant mass to the main part. As a result, the neck is thicker and does not break into satellite drops. So, in the periodic dripping regime, the formation of satellite drops is closely related to the velocity. The different stages of drop formation in the periodic dripping regime are shown on Figure 2.2.

As mentioned previously, the fluid velocity in the periodic regime is very low comparing to that of the other regimes. Because of the low flow rate, the liquid wets the edges of the nozzle; therefore the drops in the periodic regime have bigger volumes and the exterior diameter of the tube is the governing geometrical parameter. Moreover, all the drops in the periodic dripping regime have the same size, pinch off at regular time interval and have the same detachment position which is very close to the tube exit, a downstream distance of approximately one diameter.

The second regime is the dripping faucet which is characterized by a slightly higher velocity and the formation of a big drop followed by smaller ones. Figure 2.3 depicts the important phases of the dripping faucet regime and shows the formation of drops of different sizes. The dripping faucet is the transition region between dripping and jetting. It is quite particular in the sense that it has multiple periodic bifurcations. In fact, the dripping faucet can have two, three or more periods of drop formation. In this regime, successive drops have different sizes but depending on the number of periods, there is a repetition of the drop sizes. For example, if at a particular velocity, the dripping faucet has a double periodic drop formation, the first and the third drops will have the same size when the second and the fourth drops will be similar. Also, the detachment point of the drops changes from one drop to another but always stays close to the tube tip. It could be noticed that the dripping faucet is not periodic in time because the drops do not pinch off at regular time interval. So contrary to the periodic

dripping which has both periodic detachment time and drop size, the dripping faucet has only periodic bifurcations.

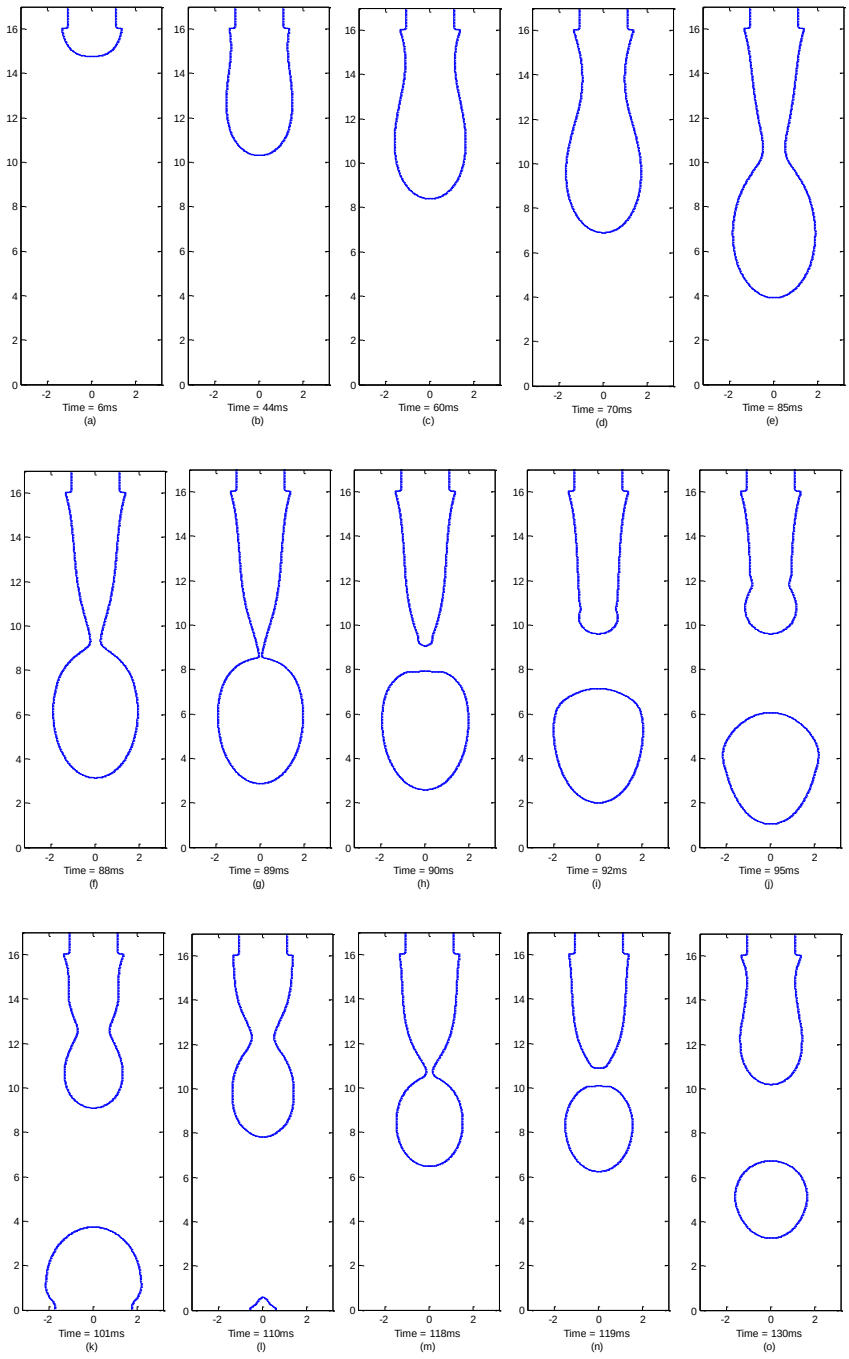

Figure 2.3 Evolution of a pendant drop from a capillary tube of inner diameter D=2.1mm and outer diameter Do=2.7mm for a liquid velocity of 0.22m/s (dripping faucet mode).

In the third regime of drop formation which the jetting, the liquid flow into the tube has a higher velocity than the other regimes. The size of the drop in the jetting mode is closely related to the velocity. For the cases investigated in the present study, the drops formed have different sizes. In fact, this paper focuses on the jetting regime with low velocity. For jetting regime with high velocity, the drops formed have the same size which is equal to the wavelength of the fastest growing wave [9]. The jetting mode studied is not characterized by periodic bifurcations like the two other regimes, so there is no repetition of drop sizes. Also the detachment point moves away from the nozzle until a long liquid column is formed (Figure 2.4). It could be noticed that the first drops of the jetting regime are formed close to nozzle tip but contrary to the other regimes of drop formation, the pinch off location of the subsequent drops changes until eventually the drops are generated from the ends of a long continuous jet. In order to have the diameter of the jet equal to the outer diameter of the tube, the incoming fluid is set to wet the nozzle exit. A wetting boundary condition at the end of the nozzle means that the fluid coming in the tube reaches its edges. However, as shown on Figure 2.1, the diameter of the jet is not uniform and is different from the outer diameter of the nozzle. The portion of the liquid column which is far from the nozzle is slender. Because of the high flow rates in the jetting regime, there is not wetting boundary condition and the exterior diameter of the tube is not longer the governing geometrical parameter.

The mechanics of drop formation in the jetting regime is very complex. When the drops are formed close to the nozzle, the process of formation is due to the loss of equilibrium between the inertial, capillary, surface tension and gravitational forces. When the length of the liquid column is long, the drops are formed due to the Plateau-Rayleigh instability [9].

The Plateau-Rayleigh instability explains why a column of liquid decomposes into drops after it reaches a certain length. There is the existence of perturbations waves in the liquid that grow with time and cause instability. In fact, all fluid streams contain perturbations, which are small changes in a physical system. These perturbations are sometimes compounded into

sinusoidal functions and appear as waves. When the waves become large enough, the liquid column pinches off and spherical droplets are formed. Theoretically, the length of the column at the brink of breaking off is equal to the wavelength of the fastest growing perturbation, which is about 9 times the column radius [9]; however, it was observed that the column could break up when its length is about 6.26 times its radius.

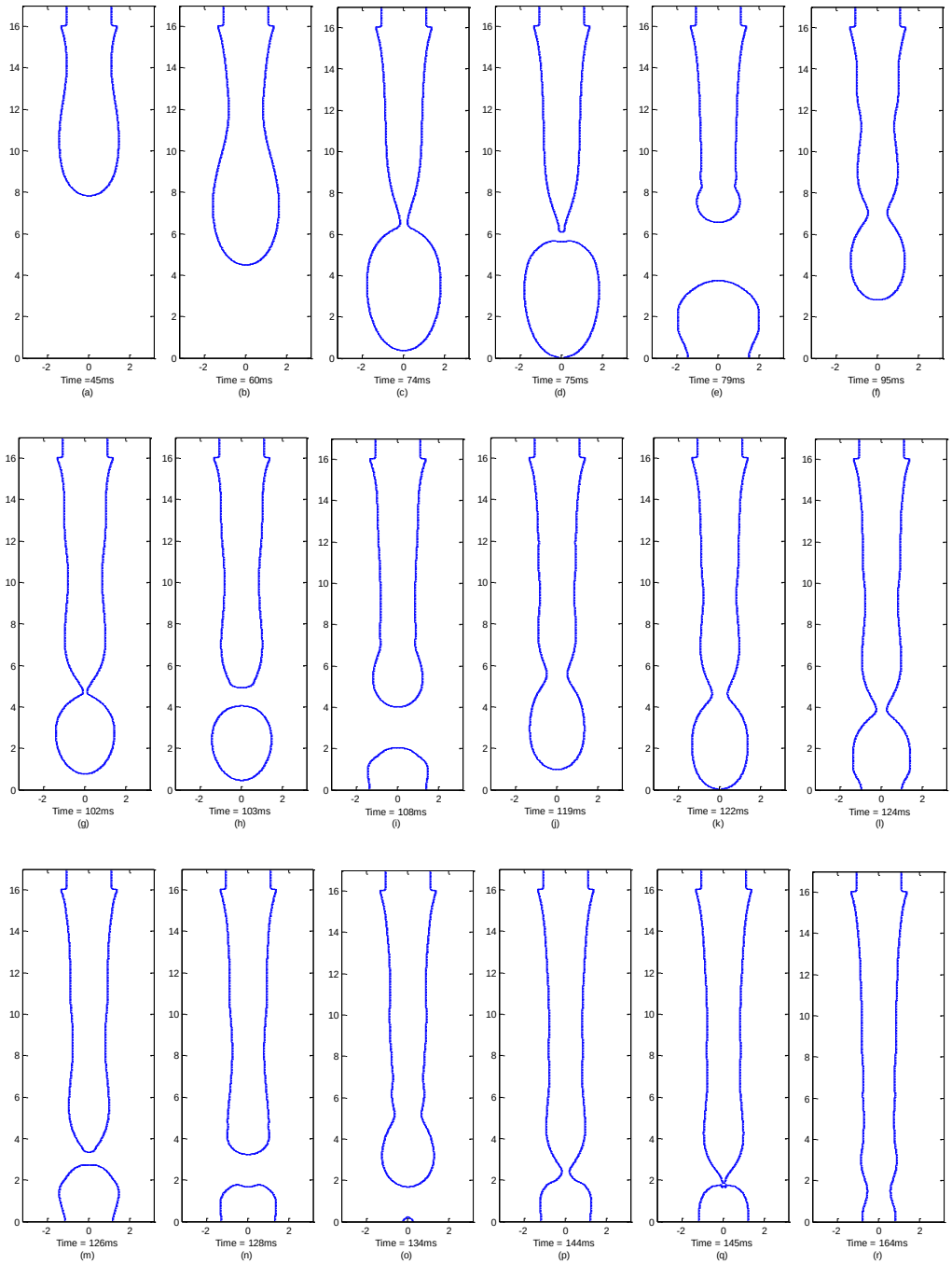

Figure 2.4 Evolution of a pendant drop from a capillary tube of inner diameter of D=2.1mm and outer diameter Do=2.7mm for a liquid velocity of 0.27m/s (jetting mode).

CHAPTER 3

NUMERICAL MODELING

3.1 Introduction

The drop formation from a capillary tube is a type of transient incompressible fluid flow problem with surface tension on the free surface. This class of problem involves a moving boundary and requires special methods to determine the free surface location. In this study, the Level Set (LS) method is used in addition to the Volume of Fluid (VOF) method for a better estimation of the free surface. The combination of the Level Set and the Volume of Fluid method is called the Couple Level Set Volume of Fluid (CLSVOF) method and was developed by Tong and Wang [15] at the University of Texas at Arlington. Once the free surface is computed, it is reconstructed with the Piecewise Linear Interface Calculation (PLIC) scheme. Originally, the free surface reconstruction method used in the code was the Nichol-Hirt (NH) algorithm which represents the interface as either horizontal or vertical lines. It was replaced by the PLIC reconstruction method which was implemented (VOF-PLIC) at The University of Texas at Arlington by Lu [16]. In the subsequent sections, a summary of the schemes used for the numerical simulation is given. The Continuum Surface Force (CSF) model is used to estimate surface tension force at the interface. The derivations of the equations in this chapter are similar to those found in [17].

3.2 Governing Equations

The computer code models a 2D fluid flow in an Eulerian frame. The governing equations are the continuity equation for incompressible flow,

$$\nabla \bullet \vec{V} = 0 \tag{3.1}$$

and the momentum equation,

$$\frac{\partial \vec{V}}{\partial t} + \nabla \bullet (\vec{V}\vec{V}) = -\frac{1}{\rho}\nabla p + \frac{1}{\rho}\nabla \bullet \tau + \vec{g} + \frac{1}{\rho}\vec{F}_b \qquad (3.2)$$

where ρ is the fluid density, p is the scalar pressure, τ is the viscous stress tensor, $\vec{F}_b$ is a body force, and $\vec{g}$ is the gravitational acceleration. For Newtonian fluid, the viscous stress tensor τ is

$$\tau = 2\nu S\,, \qquad (3.3)$$

$$S = \frac{1}{2}[(\nabla \vec{V}) + (\nabla \vec{V})^T] \qquad (3.4)$$

where S is the rate-of-strain tensor and ν is the coefficient of dynamic viscosity. The first step of the flow solving algorithm is to discretize the momentum Equation (3.2) as follows:

$$\frac{\vec{V}^{n+1} - \vec{V}^n}{\delta t} = -\nabla \bullet (\vec{V}\vec{V})^n - \frac{1}{\rho^n}\nabla p^{n+1} + \frac{1}{\rho^n}\nabla \bullet \tau^n + \vec{g}^n + \frac{1}{\rho^n}\vec{F}_b^n \qquad (3.5)$$

where the superscript (n) and (n+1) represent time step of (n) and (n+1) , respectively. The two-step projection method is used. Equation (3.5) is split in the following two steps:

$$\frac{\tilde{\vec{V}} - \vec{V}^n}{\delta t} = -\nabla \bullet (\vec{V}\vec{V})^n + \frac{1}{\rho^n}\nabla \bullet \tau^n + \vec{g}^n + \frac{1}{\rho^n}\vec{F}_b^n \qquad (3.6)$$

and

$$\frac{\vec{V}^{n+1} - \tilde{\vec{V}}}{\delta t} = -\frac{1}{\rho^n}\nabla p^{n+1} \qquad (3.7)$$

where $\tilde{\vec{V}}$ is an intermediate velocity field. In the first step, $\tilde{\vec{V}}$ is computed from the values of the previous time step: advection, viscosity, gravity, and body forces are approximated at the old time, t = n. In the second step, the intermediate velocity field is projected onto a zero-divergence vector field. Then Equations (3.7) and the discretized continuity equation

$$\nabla \bullet \vec{V}^{n+1} = 0 \quad , \qquad (3.8)$$

are combined into an pressure equation called the pressure Poisson equation (PPE),

$$\nabla \bullet [\frac{1}{\rho^n} \nabla p^{n+1}] = \frac{\nabla \bullet \tilde{\tilde{V}}}{\delta t} . \tag{3.9}$$

Equation (3.9) is solved by using an incomplete Cholesky conjugate gradient (ICCG) solution technique. Once ∇p^{n+1} is known, Equation (3.7) can be solve, giving the vector field of the next time step, t = n + 1.

3.3 Free Surface Tracking Method

In the present study, free surfaces are tracked by a method called Volume of Fluid (VOF) which was pioneered by Hirt and Nichols [18]. Free surfaces are reconstructed by using a scalar field $F(\vec{x}, t)$, which is called the VOF function and is defined as follows:

$$F(\vec{x}, t) = \begin{cases} 1, & \text{in the fluid} \\ 0 < F < 1, & \text{at the interface,} \\ 0, & \text{in the void.} \end{cases} \tag{3.10}$$

From this definition, the VOF function can be interpreted as the normalized volume fluid inside a cell. The discontinuity in *F* is a Lagrangian invariant [1], propagating according to:

$$\frac{DF}{Dt} = \frac{\partial F}{\partial t} + (\vec{V} \bullet \nabla) F = 0 . \tag{3.11}$$

The VOF method uses the donor-accepter differencing to track the movement of the free surfaces. The exact solution to Equation (3.11) would yield

$$(\frac{\partial F}{\partial t})_{exact} = -(\vec{V} \bullet \nabla) F \tag{3.12}$$

where the term exact refers to the analytical solution of the partial differential equation. The form of Equation (3.12) used for numerical purpose is the following equation:

$$(\frac{\partial F}{\partial t})_{calc} = -(\nabla \bullet \vec{V}) F - (\vec{V} \bullet \nabla) F \tag{3.13}$$

where the term calc refers to the numerical solution of the partial differential equation. By combining Equations (3.12) and (3.13), the following equation which can reduce the numerical error in the VOF advection calculation is obtained:

$$(\frac{\partial F}{\partial t})_{exact} = (\frac{\partial F}{\partial t})_{calc} + (\nabla \bullet \vec{V})F \ . \tag{3.14}$$

Splitting the above equation into two equations using an intermediate value $\tilde{F}$ in a similar manner as in the Navier-Stokes equation:

$$\tilde{F} = F^n - \delta t \nabla \bullet (\vec{V} F^n) \tag{3.15}$$

and

$$F^{n+1} = \tilde{F} + (\nabla \bullet \vec{V})F^n \ . \tag{3.16}$$

The numerical errors are corrected by this treatment for advecting F to the next time step.

In the beginning of the computational cycle, fluid volumes are initialized in each cell according to the free surface geometry. Then the interface is discretized to proceed the calculation and the discrete fluid volume data is utilized for further computations. This discrete volume data is used to reconstruct an interface of the fluid. In the present study, a free surface reconstruction algorithm known as Piecewise Linear Interface Calculation (PLIC) is used. It reconstructs the free surface interface as a linear line segment with an angular orientation in such a way that the fraction of the fluid volume in each cell is equal to F . The Nichol-Hirt (NH) algorithm, which is the original reconstruction algorithm of RIPPLE, reconstructs the interface in each cell either horizontally or vertically, making use of the actual interface normal and the cell neighbors. The PLIC algorithm has been demonstrated to show less distortion than the NH algorithm [16].

3.4 Surface Tension Model

Surface tension at free surface is modeled with a non-conventional approach called Continuum Surface Force (CSF) method which was proposed by Brackbill, Kothe and Zemach

[19]. Viscous effects are neglected at the free surface and the surface tension coefficient is assumed to be constant: the surface force has no tangential component. Therefore, the surface stress boundary condition at a free surface is reduced to the Laplace's formula

$$p_s \equiv p - p_v = \sigma\kappa \tag{3.17}$$

where p_s is the surface pressure jump induced by surface tension, p_v is the vapor pressure, σ is the surface tension coefficient of the fluid, and κ is the local free surface curvature. The curvature can be calculated as follows:

$$\kappa = -(\nabla \bullet \hat{n}) \tag{3.18}$$

where $\hat{n}$ is the unit normal vector given by:

$$\hat{n} = \frac{\vec{n}}{|\vec{n}|}. \tag{3.19}$$

In the above equation, the normal vector $\vec{n}$ is expressed as

$$\vec{n} = \nabla\Phi \tag{3.20}$$

where Φ is a scalar field which is used to represent a free surface interface. In the CSF model, a volume force $\vec{F}_{sv}$ acts on fluid elements lying within the finite thickness transition region replacing the discontinuities. In the transition region, force density is defined to be proportional to the local curvature, thus the volume force is given by

$$\vec{F}_{sv}(\vec{x}) = \sigma\kappa(\vec{x})\frac{\nabla\tilde{c}(\vec{x})}{[c]} \tag{3.21}$$

where $\tilde{c}$ is the "color" function which serves as a material identifier and $[c]$ is the normalizing factor which is equal to 1. In the present study, $\tilde{c}$ is equivalent to Φ in Equation (3.20). Note that surface tension force, which is a surface force, is transformed into a body force in the Navier-Stokes equation i.e.

$$\vec{F}_b = \vec{F}_{sv} \ . \tag{3.22}$$

Therefore, the CSF model makes use of the fact that numerical models of discontinuities are really continuous transitions within which the fluid properties vary smoothly from one fluid to another.

The VOF-NH scheme, which is the original scheme in RIPPLE, adopts the NH algorithm for the free surface reconstruction. The VOF-PLIC scheme uses the PLIC method for its reconstruction and when compared with the VOF-NH scheme, it offers better surface reconstruction [16]. In those VOF schemes, the scalar function in Equation (3.20) is equivalent to the VOF function, $F(\vec{x},t)$.

The CLSVOF scheme is a hybrid scheme for the free surface tracking. It adopts the VOF method for the volume tracking, Equation (3.11), and the Level Set (LS) method for the estimation of the local curvature and normal vector to the free surface. The LS method is introduced since the VOF method shows good mass conservation property but lacks the accuracy in the computation of the local curvature and the normal vector. This problem arises from the nature of the VOF function, $F(\vec{x},t)$, which is a discontinuity function. The LS function is defined as a distance function as follows:

$$\phi(\vec{x},t)\begin{cases} > 0, & \text{outside of the interface,} \\ = 0, & \text{at the interface,} \\ < 0, & \text{inside the interface.} \end{cases} \tag{3.23}$$

This function is evolved by

$$\frac{D\phi}{Dt} = \frac{\partial\phi}{\partial t} + (\vec{V} \bullet \nabla)\phi = 0 . \tag{3.24}$$

To keep the LS function ϕ a distance function, a re-initialization process is required [20]:

$$\frac{\partial\phi}{\partial\tau} = \frac{\phi_0}{\sqrt{{\phi_0}^2 + h^2}}(1 - |\nabla\phi|) \tag{3.25}$$

where ϕ_0 is the level set function of the previous time step, τ is the artificial time, and h is the grid width. Since the scalar field Φ is equivalent to the LS function ϕ, the normal vector in Equation (3.20) can be written as

$$\vec{n} = \nabla\phi \tag{3.26}$$

and therefore, Equation (3.19) becomes

$$\hat{n} = \frac{\nabla\phi}{|\nabla\phi|} = \nabla\phi \tag{3.27}$$

where $|\nabla\phi| = 1$. The local curvature of the free surface interface (3.18) becomes

$$\kappa = -\nabla \bullet \nabla\phi \ . \tag{3.28}$$

While the VOF function is a jump function, the LS function is a smooth function thus it is expected to show better accuracy in taking the gradient of the function. Therefore, it is reasonably presumed that the CLSVOF shows better results in the free surface simulation. A graphical overview of the CLSVOF scheme is shown in Figure 3.1. The only disadvantage of this scheme is that it imposes more computational loads since the scheme calculates both the VOF and LS function.

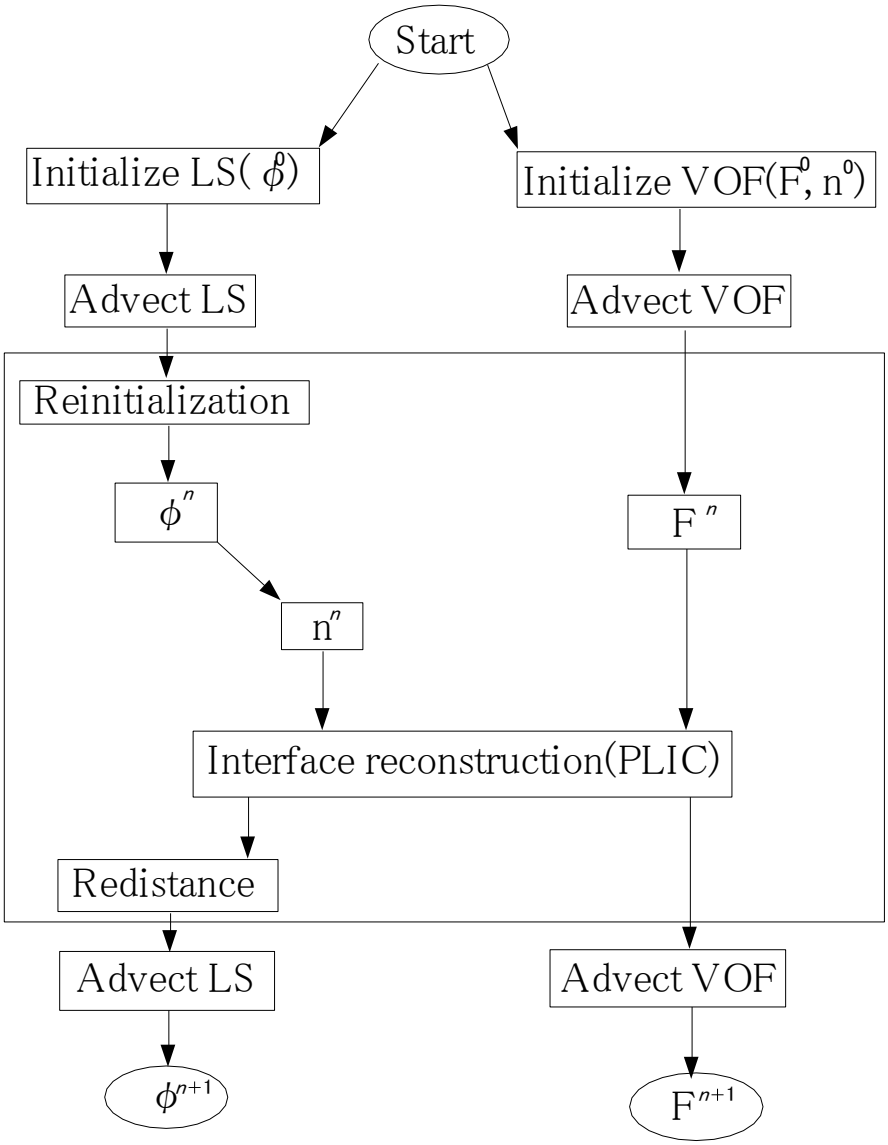

Figure 3.1 Overview of the CLSVOF scheme

CHAPTER 4

RESULTS AND DISCUSSION

4.1 Introduction

As stated previously, this study is a numerical simulation and the computer program used is a version of RIPPLE to which was added the Level Set (LS) and PLIC schemes for a better modeling of the free surface. The velocity of the fluid, the inner and outer diameters of the capillary tube are varied to generate the various regimes of drop formation from dripping to jetting and to determine the limits of those regimes. Once the different regimes have been found, their main characteristics will be examined. Then the mechanism of drop formation in each regime is explained by showing the action of different forces and instabilities. Matlab is used to post-process the data and the numerical results are compared with experimental data reported in the literature [2].

The numerical simulations were done with five different tube diameters. The dimensions of the nozzle were taken from the empirical data reported by Clanet and Lasheras [2]. Every nozzle is characterized by a set of dimensions formed by the inner diameter D and the exterior diameter Do which are related to each other by a third order polynomial approximation. The sets are called cases and numbered from 1 to 5 (Table 4.1).

Table 4.1 Diameters Used in Numerical and Experimental Studies

	Diameters used for simulation (mm)		Diameters used in experiment (mm)		
	D	Do	D	Do	Grid size (dr)
Case1	0.832	1.216	0.838	1.27	0.032
Case2	1.152	1.6	1.19	1.65	0.032

Table 4.1 - *Continued*

Case3	1.6	2.1	1.6	2.11	0.05
Case4	2.1	2.7	2.16	2.77	0.05
Case5	4.1	4.7	4.1	4.75	0.05

For every case, the inlet velocity is varied and sub-cases are obtained. There are about six sub-cases for every case. The velocities in the sub-cases are selected such that the limits between the different regimes could be easily determined.

The actual dimensions used in the computer simulation differ slightly from that of [2]. In this study, the drop formation is an axi-symmetric problem and only half of the domain is calculated. The radius of the tube used for the simulation has to be a multiple of the grid size in the radial direction, so that the number of cells is an integer. Table 4.1 shows the grid size (dr) used for the simulation and the dimensions of the nozzle used in the experimental [2] and numerical studies. Note that the diameters used in the simulations are slightly smaller than the ones used for the experiments [2]. Also for the smaller nozzles (Case1 & 2), a smaller grid size is used for better resolution.

In order to generate the different regimes, the inlet velocity is gradually increased until the limits between the regimes are reached. The velocity limit is dependent on the nozzle diameter. The working fluid used in the present study is water at 20 $^{\circ}C$ and its physical properties are as follows:

Kinematic Viscosity (υ) = 10^{-6} m^2/s

Density (ρ) = 1000 kg/m^3

Surface Tension Coefficient (σ) = 7.3 $\times 10^{-2}$ N/m.

The cylindrical coordinate is used in the simulation. The capillary tube is modeled as an interior obstacle or non-flow region [1]. The initial shape of the liquid in the tube is represented

by a series of free surface conic functions (Figure 4.1). Axi-symmetrical calculations are done to save computational resources.

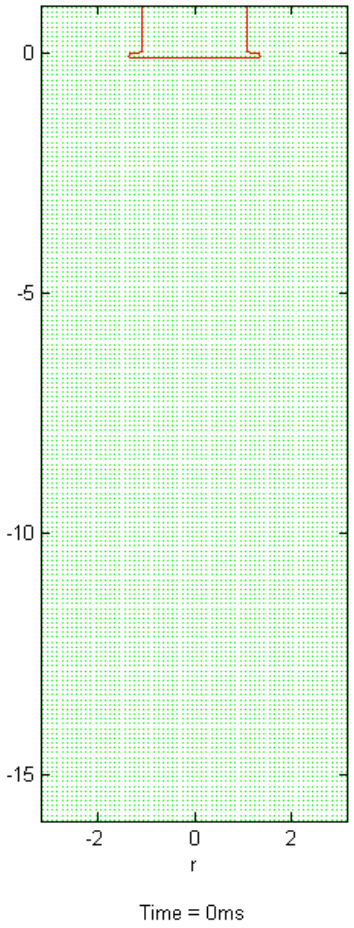

Figure 4.1 Initial shape of the water droplet

The boundary condition at the inner tube wall is nonslip and without penetration, i.e. $v_r = v_z = 0$. In accordance to the experimental requirements, the fluid initially at rest wets the tube exit section and the velocity profile of the incoming flow is fully developed parabolic. A wet boundary condition in the present study is obtained by filling only the one cell located on the edge of the front surface of the capillary tube.

4.2 Comparison of Numerical and Experimental Studies

The numerical study is performed with five different nozzle diameters with the velocity magnitude gradually increased for each case. A summary of the results is given in Table 4.2. It should be noticed from the cases studied that the bigger the diameter of the nozzle, the bigger the drop volume and the longer the pinch off time. For every set of nozzle diameters Do (outer diameter) and D (inner diameter), as the velocity increases, there is first the periodic dripping regime, then the dripping faucet regime and finally the jetting regime.

In order to characterize the regimes, the Weber number, We (Equation 4.1), a dimensionless number which measures the relative importance of the fluid's inertia compared to its surface tension, will be used in addition to the velocity. The Weber number is defined as:

$$We = \frac{\rho v^2 D}{\sigma} \qquad 4.1$$

where ρ is the fluid density, D is the inner diameter of the tube, v is the fluid velocity, and σ is the fluid surface tension.

For lower Weber number, there is the periodic dripping regime which is characterized by a periodic detachment of the drop. For a given velocity, the drops have the same volume and they pinch off at regular time interval, at positions very close to the nozzle tip. The drop size decreases with the increase of the velocity.

By increasing the Weber number, the dripping faucet is reached. In this regime, there are multiple periods of drop detachment. Successive drops with different sizes and detachment periods are generated (Table 4.2). The bifurcation pattern of the dripping faucet regime differs from one case to another, and it is quite difficult to predict when there will be a double or a triple period; however the pinch off position always stays close to the tube exit.

The last regime is the jetting which has a higher Weber number than the dripping faucet. In the jetting regime, the detachment points of the drops are much lower comparing to that of the other regimes. When the velocity in the jetting regime is very close to the transition

velocity, the first drops are formed very close to the nozzle tip then the detachment point moves downstream, away from the nozzle tip. For very high velocity, the first drops are formed very far from the tube exit, at a distance of about 10D [2]. In the present study, the focus was not on the jetting regime with very high velocity; and because of the limit on the length of the computational domain, the formation of drops very far from the tip of the nozzle was not studied.

One objective of this study is to observe the drop formation in the different regimes; this goal was reached by running the cases and providing qualitative and quantitative descriptions. The other objective is to determine the velocity limits between those regimes and compare them to available empirical data.

The numerical and experimental data are compared by studying two different graphs (Figures 4.2 and 4.3). Figure 4.2 is from [2] and represents only the experimental results.

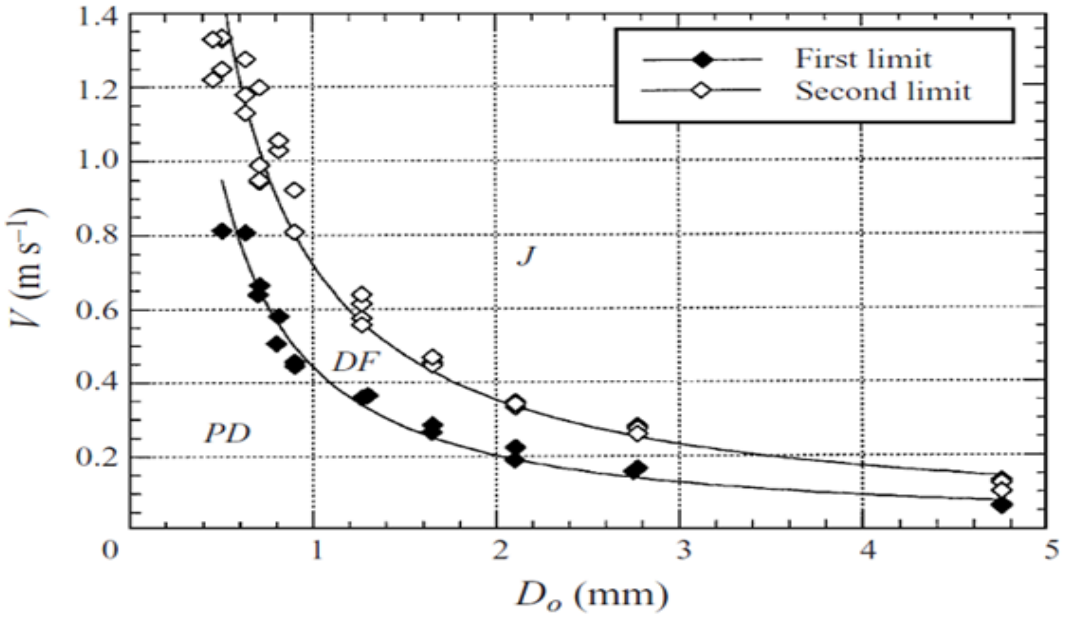

Figure 4.2 Boundaries of the different regimes of drop formation [2]

On Figure 4.2, there is the representation of the two velocity limits versus the nozzle outer diameter. The first limit is between the periodic dripping and the dripping faucet, while the

second limit is between the dripping faucet and the jetting mode. The markers are the experimental data and the straight lines are the curve fit. That graph is very useful for it permits to predict the regime of drop formation for a given diameter and velocity. It could be noticed that for smaller diameters, the periodic dripping exists over a wide velocity range. In many applications, it is critical to have uniform drop sizes and regular pinch off time; so knowing the velocity range of the periodic dripping is very important.

Figure 4.3 shows both experimental and numerical results. The data points represent the numerical results and the lines are the exported experimental regression curves [2].

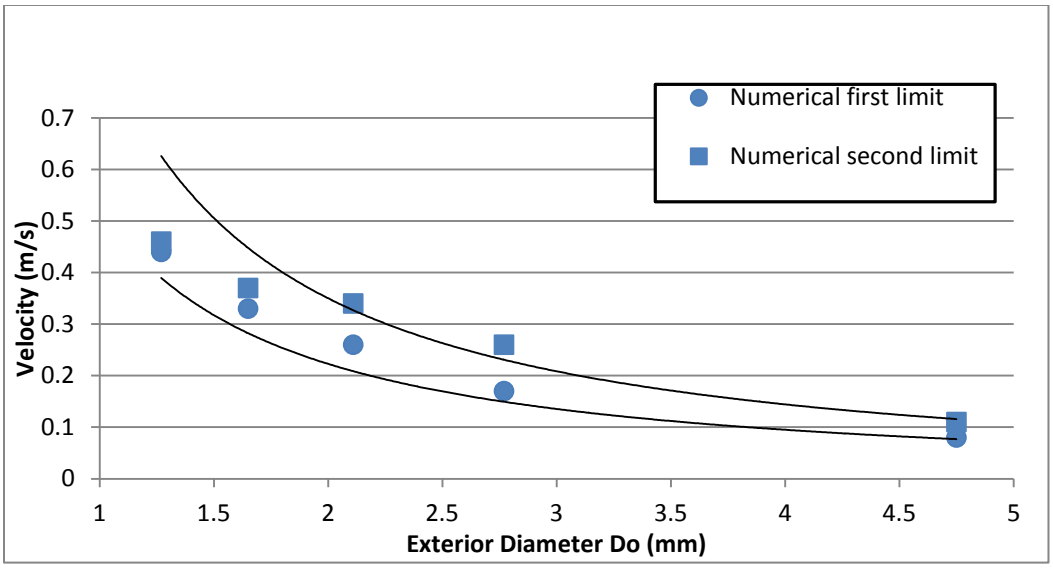

Figure 4.3 Velocity limits versus exterior diameter: data points – numerical limits; lines – experimental limits [2]

Although both limits obtained by experiment and numerical simulations are very close, a difference could be noticed. In fact, the numerical first limit is higher than the experimental one and this means that to reach the numerical first limit, a higher velocity is needed. However the numerical second limit is lower than the empirical one, which means that for a lower velocity, there is jetting for the numerical simulation.

Figure 4.3 gives a visual representation of the difference between the numerical and experimental data. In order to have a better appreciation of the difference between those two types of data, a qualitative analysis is done. Table 4.3 gives a summary of the different cases run and shows the numerical and experimental velocity limits and the percentage error. It could be observed from Table 4.3 that there is a difference between the numerical and experimental limits and this difference is expressed by the percentage error which shows how the numerical results differ from the experiments The error percentage varies from one nozzle diameter to the other.

For the smallest diameter there is a greater percentage of error for both first and second limits. This could be due to the fact that to study the dripping for tube of very small diameters, the grid size used during the simulation needs to be very fine. This creates some issues because of the memory size of the numerical tool.

Also there is a higher percentage of error for the first limit because the limit between the periodic dripping and dripping faucet is very difficult to catch. In the periodic dripping regime, all the drops have the same volume when in the dripping faucet regime, successive drops are different. In fact one of the differences between those regimes is that for the dripping faucet, there is the formation of a smaller drop after the first one; and when the velocity is not too high, the smaller drop is almost similar to the primary one, making it harder to determine where one regime stops and the other starts.

Another source of error may be due to the changes made for the simulations. For example, the diameters used for numerical simulation are taken from the experimental data. However, those diameters are slightly modified because the dimensions used for the simulation have to be a multiple of the grid size, so that the number of the cells is an integer.

Table 4.2 Summary of the Different Cases Run

						Drop formation Time						
	D	Do	Velocity	Weber No.	dr	1st Drop	2nd Drop	3rd Drop	4th Drop	5th Drop	Flow rate	Description
	mm	mm	m/s		mm	ms	ms	ms	ms	ms	ml/min	
Case1_V1	0.832	1.216	0.35	1.40	0.032	67	63	66	64	63	11.4	Periodic dripping (no satellite drop)
Case1_V2	0.832	1.216	0.41	1.92	0.032	43	36	36	34	36	13.4	Periodic dripping (no satellite drop)
Case1_V3	0.832	1.216	0.43	2.11	0.032	37	32	30	32	22	14.0	Periodic dripping (no satellite drop)
Case1_V4	0.832	1.216	0.45	2.31	0.032	33	15	24	13	31	14.7	Dripping faucet (two periods)
Case1_V5	0.832	1.216	0.47	2.52	0.032	31	38	16	14	10	15.3	Jetting (detachment moving lower)
Case2_V1	1.152	1.60	0.25	0.99	0.032	85	80	80	80	80	15.6	Periodic dripping (no satellite drop)
Case2_V2	1.152	1.60	0.30	1.42	0.032	63	53	52	53	52	18.8	Periodic dripping (no satellite drop)
Case2_V3	1.152	1.60	0.32	1.62	0.032	55	58	43	24	49	20.0	Periodic dripping (no satellite drop)
Case2_V4	1.152	1.60	0.34	1.82	0.032	50	17	46	19	33	21.3	Dripping faucet (two periods with a big drop and slightly smaller one)
Case2_V5	1.152	1.60	0.36	2.05	0.032	47	17	28	14	31	22.5	Dripping faucet (two periods with a big drop and very smaller one)
Case2_V6	1.152	1.60	0.38	2.28	0.032	45	17	30	14	16	23.8	Jetting

Table 4.2 - *Continued*

case3_V1	1.60	2.10	0.15	0.49	0.05	123	103	105	104	105	18.1	Periodic dripping (no satellite drop)
case3_V2	1.60	2.10	0.25	0.88	0.05	92	71	72	72	72	24.1	Periodic dripping (no satellite drop)
case3_V3	1.60	2.10	0.27	1.60	0.05	84	49	67	53	67	32.6	Dripping faucet (multiple drop sizes)
case3_V4	1.60	2.10	0.29	1.84	0.05	76	28	63	28	52	35.0	Dripping faucet (multiple drop sizes)
case3_V5	1.60	2.10	0.3	1.97	0.05	73	30	33	27	64	36.2	Dripping faucet (three periods)
case3_V6	1.60	2.10	0.31	2.11	0.05	71	22	44	27	55	37.4	Dripping faucet (multiple drop sizes)
case3_V7	1.60	2.10	0.33	2.39	0.05	67	26	18	22	19	39.8	Dripping faucet (multiple drop sizes)
case3_V8	1.60	2.10	0.34	2.53	0.05	66	27	20	18	17	41.0	Jetting
Case4_V1	2.10	2.70	0.08	0.18	0.05	241	209	210	209	210	16.6	Periodic dripping (satellite drop)
Case4_V2	2.10	2.70	0.15	0.65	0.05	134	110	108	114	106	31.2	Periodic dripping (no satellite drop)
Case4_V3	2.10	2.70	0.2	1.15	0.05	100	55	39	68	39	41.5	Dripping faucet (three periods)
Case4_V4	2.10	2.70	0.22	1.39	0.05	89	30	54	25	63	45.7	Dripping faucet (two periods)
Case4_V5	2.10	2.70	0.23	1.52	0.05	84	28	49	28	43	47.8	Dripping faucet (two periods)
Case4_V6	2.10	2.70	0.25	1.80	0.05	78	27	22	23	28	51.9	Dripping faucet (multiple drop sizes)
Case4_V7	2.10	2.70	0.27	2.10	0.05	75	28	23	---	---	56.1	Jetting (not pattern and pinch off position moves down)

Table 4.2 - *Continued*

Case5_V1	4.10	4.70	0.018	0.02	0.05	474	364	358	347	334	14.3	Periodic dripping (satellite drop)
Case5_V2	4.10	4.70	0.05	0.14	0.05	216	131	160	142	162	39.6	Periodic dripping (no satellite drop)
Case5_V3	4.10	4.70	0.06	0.20	0.05	191	125	122	122	141	47.5	Periodic dripping (no satellite drop)
Case5_V4	4.10	4.70	0.07	0.28	0.05	174	113	118	120	106	55.4	Periodic dripping (no satellite drop)
Case5_V5	4.10	4.70	0.08	0.36	0.05	159	67	111	87	68	63.3	Dripping faucet (multiple drop sizes)
Case5_V6	4.10	4.70	0.09	0.45	0.06	149	52	80	100	77	71.3	Dripping faucet (multiple drop sizes)
Case5_V7	4.10	4.70	0.1	0.56	0.06	140	49	48	66	95	79.2	Dripping faucet (multiple drop sizes)
Case5_V8	4.10	4.70	0.12	0.81	0.06	124	46	30	28	------	95.0	Jetting

Table 4.3 Experimental and Numerical Velocity Limits and the Percentage of Error

	Numerical Limits (m/s)		Experimental Limits (m/s)		Percentage Error	
Do (mm)	First Limit	Second Limit	First Limit	Second Limit	First Limit	Second Limit
1.27	0.44	0.46	0.36	0.60	22.22	23.00
1.65	0.33	0.37	0.28	0.45	17.86	17.00
2.11	0.26	0.34	0.22	0.33	18.18	3.03
2.77	0.17	0.26	0.17	0.25	0.00	4.00
4.75	0.08	0.11	0.07	0.11	14.29	0.00

4.3 Effect of the Viscosity

Parametric study is done to observe the effect of viscosity of the fluid on the limits between the regimes. The nozzle with dimensions D=1.60 mm and Do=2.10 mm is chosen for the study. The viscosity is increased from $2.008*10^{-3}$ to $12.0*10^{-3}$ m^2/s. For all the sub-cases, Table 4.4 shows the velocity, the viscosity, the regime of drop formation and the volume of the drops.

Table 4.4 Effect of the Viscosity

					Normalized drop volume					
	Velocity	Viscosity	Regime of formation	Vnorm	1st	2nd	3rd	4th	5th	6th
	m/s	10-3 m2/s		mm^3						
Case3_V2_vis	0.25	2	Periodic Dripping	32.72	104	100	98	99	98	99
Case3_V2_vis2	0.25	4	Periodic Dripping	33.68	105	100	100	100	100	100
Case3_V2_vis3	0.25	6	Periodic Dripping	36.11	103	100	102	102	102	102

Table 4.4 - *Continued*

Case3_V2_vis4	0.25	12	Periodic Dripping	43.87	97	100	100	100	100	100
Case3_V3_vis	0.27	2	Dripping Faucet	32.97	98	100	95	75	94	70
Case3_V3_vis2	0.27	4	Periodic Dripping	33.62	100	100	103	105	105	
Case3_V3_vis3	0.27	6	Periodic Dripping	33.94	105	100	99	99	99	99
Case3_V3_vis4	0.27	12	Periodic Dripping	39.55	104	100	101	101	101	101
Case3_V4_vis	0.29	2	Dripping Faucet	30.85	100	53	98	48	95	55
Case3_V4_vis2	0.29	4	Dripping Faucet	32.04	100	88	102	58	98	81
Case3_V4_vis3	0.29	6	Periodic Dripping	35.31	95	100	105	103	104	103
Case3_V4_vis4	0.29	12	Periodic Dripping	37.15	106	100	100	100	100	100
Case3_V5_vis	0.31	2	Dripping Faucet	29.08	100	42	71	65	98	45
Case3_V5_vis2	0.31	4	Dripping Faucet	30.21	100	54	102	54	101	54
Case3_V5_vis3	0.31	6	Dripping Faucet	31.66	100	77	109	72	109	
Case3_V5_vis4	0.31	12	Periodic Dripping	38.04	99	100	103	104	104	104
Case3_V6_vis	0.33	2	Dripping Faucet	27.69	100	43	54	66	76	43
Case3_V6_vis2	0.33	4	Dripping Faucet	28.9	100	47	92	60	73	53
Case3_V6_vis3	0.33	6	Dripping Faucet	29.92	100	55	63	90	70	78
Case3_V6_vis4	0.33	12	Periodic Dripping	37.93	93	100	103	98	104	94
Case3_V7_vis	0.35	2	Jetting	11.61	233	100	118	103	113	96
Case3_V7_vis2	0.35	4	Jetting	12.62	220	100	123	115	115	114
Case3_V7_vis3	0.35	6	Jetting	15.07	190	100	109	99	94	81
Case3_V7_vis4	0.35	12	Jetting	21.76	153	100	97	94		

The volume of the drops is normalized for a better examination. The normalization shows clearly the difference between the drop sizes because the volume of the drops is expressed in function of the volume of one particular drop. For the periodic dripping regime, the volume of the second drop is used for the normalization because most of the time, the first drop is slightly bigger than the other drops. For the other two regimes, the volume of the first drop is used for the normalization. The volume used for normalization in the different tables is named Vnorm. From Table 4.4, it could be noticed that in the periodic dripping regime, the drops have

almost the same size. One of the main characteristics of the dripping faucet is the change of the volume of successive drops. Clanet and Lasheras [2] quantify this change and state that if the volume change between the different drops is more than 20%, the regime of drop formation is the dripping faucet. The same criterion is used in the present study to determine the dripping faucet regime. In Table 4.4, if the difference between the normalized volumes is more than 20%, the regime of drop formation for those particular sub-cases is the dripping faucet.

The viscosity affects the velocity limit between the periodic dripping and the dripping faucet but it has little impact on the jetting regime. It could be noticed from Table 4.4, that the velocity for jetting does not change even with the increase of the viscosity. As the viscosity increases, the velocity limit between the periodic dripping and the dripping faucet increases and since the velocity limit between the dripping faucet and the jetting is not affected; therefore, the velocity range over which the dripping faucet exists is reduced. For very high viscosity, there is not dripping faucet [10]. As the velocity of the fluid is increased, the regime of drop formation goes directly from periodic dripping to jetting. This fact could be observed in Table 4.4, where there is not dripping faucet regime for the sub-case with the highest viscosity.

The viscosity affects the size and pinch off time of the drop in the periodic dripping regime. Table 4.5 shows different sub-cases where all the parameters are kept constant except for the viscosity.

Table 4.5 Effect of the Viscosity for a Fluid Velocity of 0.25 m/s

				Drop detachment time				Drop volume			
	Velocity	Viscosity	Regime	1st	2nd	3rd	4th	1st	2nd	3rd	4th
	m/s	10-3 m2/s		s				mm^3			
Case3_V2_vis	0.25	2	Periodic Dripping	92	73	73	73	34.04	32.72	32.18	32.4
Case3_V2_vis2	0.25	4	Periodic Dripping	94	76	76	76	35.42	33.68	33.68	33.7
Case3_V2_vis3	0.25	6	Periodic Dripping	97	82	82	84	37.32	36.11	36.69	36.7
Case3_V2_vis4	0.25	12	Periodic Dripping	109	98	100	100	42.44	43.87	43.91	43.89

In order to better compare the volume and detachment time of the drops, the velocity for the different sub-cases is selected such that the regime of drop formation is the periodic dripping. As the viscosity increases, the drops formed have more volume and take more time to detach.

The formation of a drop is affected by the detachment of the previous drop. In fact, after the pinch off of a drop, there is the creation of ripples that affects the mechanism of formation of subsequent drops. The greater the effect of the ripples, the less time it will take the following drop to form. The primary drop is not affected and takes more time to form. The viscosity tends to damp the action of the ripples and as the viscosity increases, the time of formation of the secondary drops becomes very close to that of the primary drop. It could be noticed from Table 4.5 that it takes more time for the first drop to form, but as the viscosity increases, the time of drop formation of subsequent drops becomes close to that of the first drop.

4.4 Effect of the Surface Tension

The surface tension plays a major role in the formation of drops. Simulations were run with different surface tension coefficients to observe the effects of the surface tension on the regimes of drop formation. Table 4.6 gives a summary of the results.

Table 4.6 Effect of the Surface Tension

					Normalized drop volume			
	Velocity	Surface Tension	Regime	Vnorm	1st	2nd	3rd	4th
	m/s	N/m		mm^3				
Case3_V3	0.25	0.0727	Periodic Dripping	32.18	105	100	99	98
Case3_V1_Surf0.5	0.1	0.0363	Periodic Dripping	20.24	104	100	100	100
Case3_V6_surf	0.31	0.1095	Periodic Dripping	45.25	102	100	101	101
Case3_V11_surf2	0.4	0.1454	Periodic Dripping	45.87	108	100	99	100
Case3_V17_surf3	0.67	0.3635	Periodic Dripping	83.38	104	100	100	100
Case3_V4	0.27	0.0727	Dripping Faucet	30.57	100	50	101	46
Case3_V2_Surf0.5	0.2	0.0363	Dripping Faucet	18.93	100	44	74	87

Table 4.6 - *Continued*

Case3_V9_surf	0.39	0.1095	Dripping Faucet	39.62	100	65	101	47
Case3_V12_surf2	0.44	0.1454	Dripping Faucet	43.98	100	44	100	61
Case3_V18_surf3	0.75	0.3635	Dripping Faucet	62.55	100	50	73	53
Case3_V8	0.34	0.0727	Jetting					
Case3_V3_Surf0.5	0.27	0.0363	Jetting					
Case3_V12_surf	0.44	0.1095	Jetting					
Case3_V13_surf2	0.48	0.1454	Jetting					
Case3_V20_surf3	0.85	0.3635	Jetting					

For each case run with a particular surface tension coefficient, three regimes of drop formation were obtained. For the periodic dripping, all the drops have sensibly the same size. For the dripping faucet, there is an alternation between big and small drops. For the jetting regime, there was not formation of drop observed because of the limit on the length of the domain of simulation. The surface tension affects both limits between the three regimes of drop formation contrary to the viscosity which only affects the limit between the periodic dripping and the dripping faucet regimes. As the surface tension coefficient increases, the velocities to reach the dripping faucet and jetting regimes also increase. The surface tension forces tend to increase the cohesion between the particles on the free surface of the system and compete against the gravitational and inertial forces for equilibrium. As it could be seen in Table 4.7, when the surface tension coefficient is increased, the volume and the detachment time of the drop increase sharply.

Table 4.7 Effect of the Surface Tension for a Fluid Velocity of 0.34 m/s

			Drop Detachment Time			Drop Volume		
	Velocity	Surface Tension	1st	2nd	3rd	1st	2nd	3rd
	m/s	N/m	s			mm^3		
Case3_V8_surf	0.34	0.1095	83	151	221	41.88	40.64	42.39
Case3_V8_surf2	0.34	0.1454	113	212	313	61.95	60.05	60.10
Case3_V8_surf3	0.34	0.3635	215	425	641	168.00	168.8	169.4

4.5 Effect of the Density

The importance of the density of the fluid on the limits between the regimes is studied by running simulations with different values of density. The nozzle with dimensions D=1.60 mm and D_0=2.10 mm is chosen for the study. Table 4.8 shows the details of the results obtained.

Table 4.8 Effect of the Density

					Normalized drop volume			
	Velocity	Density	Regime	Vnorm	1st	2nd	3rd	4th
	m/s	kg/dm^3						
Case3_V3	0.25	1	Periodic Dripping	32.18	105	100	99	98
Case3_V10_dens0.5	0.38	0.5	Periodic Dripping	52.26	103	100	102	100
Case3_V1_dens2	0.1	2	Periodic Dripping	20.27	104	100	-	-
Case3_V4	0.27	1	Dripping Faucet	30.57	100	50	101	46
Case3_V12_dens0.5	0.42	0.5	Dripping Faucet	46.53	100	67	93	45
Case3_V2_dens2	0.2	2	Dripping Faucet	18.95	100	44	73	88
Case3_V8	0.34	1	Jetting	28.06	100	41	44	-
Case3_V15_dens0.5	0.5	0.5	Jetting	40.47	100	48	52	-
Case3_V3_dens2	0.25	2	Jetting	18.4	100	42	-	-

The density not only affects the velocity limit between the periodic dripping and the dripping faucet, but it also has an impact on the velocity limit between the dripping faucet and the jetting. As the density increases, the velocities to reach the dripping faucet and jetting regimes decrease. The density affects the size and pinch off time of the drops in the three regimes. From Table 4.8, it could be observed that the higher the density, the smaller the volume of the drops. This fact is also demonstrated in Table 4.9 where all the parameters are kept constant except for the density. As the density increases, the drops formed have less volume and detach rapidly.

Table 4.9 Effect of the Density for a Fluid Velocity of 0.10 m/s

				Drop detachment time			Drop volume		
	Velocity	Density	Regime	1st	2nd	3rd	1st	2nd	3rd
	m/s	kg/dm^3		s			mm^3		
Case3_V1	0.1	1	Periodic Dripping	157	297	436	40.16	39.42	39.45
Case3_V1_dens0.5	0.1	0.5	Periodic Dripping	162	314	466	72.46	73	73.14
Case3_V1_dens2	0.1	2	Periodic Dripping	143	258	373	21.16	20.27	20.30

4.6 Convergence Study

Space and time convergences study have been done to validate the numerical results. Simulations were run using different grid sizes and it was found that there was a range of grid size over which meaningful results were obtained. That range changes for every nozzle diameter. For small diameters, the grid size had to be less than 0.032mm for accurate results when for bigger diameters, a grid size close to 0.05mm was fine. Table 4.1 shows the grid size chosen for the different nozzle. Those grid sizes were the ones that save computational time while giving good results. Grid refinement was tested by running two simulations with different grid sizes. In order to conserve the dimensions of the nozzle for a particular case, the grid size for the second simulation was chosen to be twice that of the first one. The result of the second simulation was not accurate and is not mentioned in the present study.

In addition to the grid refinement study, a time convergence has been performed. The computer code requires three time step constraints for stability [1]. They are the viscous, Courant, and capillary conditions and the code adjusts the time step automatically according to these constraints. However, the adjusted time step is only sufficient for the stability and it does not guarantee the accuracy of the calculation especially a flow simulation with strong capillary effect. The parameter *dtmax* in the *input* file denotes the maximum time step allowed in the calculation and more accurate results can be obtained by reducing this number [17]. Table 4.10

shows simulations with two *dtmax values*. The results for the different simulations are very similar except in the two last cases where the detachment time differs.

Table 4.10 Time Convergence Summary

						Drop Detachment Time					
	D	Do	Velo -city	dr	*dtmax*	1st Drop	2nd Drop	3rd Drop	4th Drop	5th Drop	Description
	mm	mm	m/s	10^{-2} mm	10^{-3} ms	ms	ms	ms	ms	ms	
Case1_V2	0.832	1.216	0.41	3.2	1.47	43	79	115	149	185	Periodic Dripping with no satellite
Case1_V2C	0.832	1.216	0.41	3.2	1.00	43	79	115	149	185	Periodic Dripping with no satellite
Case1_V3	0.832	1.216	0.43	3.2	1.47	37	69	99	131	153	Periodic Dripping with no satellite
Case1_V3C	0.832	1.216	0.43	3.2	1.00	37	69	99	131	155	Periodic Dripping with no satellite
Case1_V4	0.832	1.216	0.45	3.2	1.47	33	48	72	85	116	Dripping faucet with a big drop and slightly smaller one
Case1_V4C	0.832	1.216	0.45	3.2	1.00	33	48	73	87	112	Dripping faucet with a big drop and slightly smaller one
Case1_V5	0.832	1.216	0.47	3.2	1.47	31	69	85	99	109	jetting with detachment point moving lower
Case1_V5C	0.832	1.216	0.47	3.2	1.00	31	65	101	119	131	jetting with detachment point moving lower

4.7 Mechanism of Drop Formation in the Different Regimes

4.7.1 Periodic Dripping

The periodic dripping is the first regime of drop formation and it has the lowest velocity. For this case, the detachment point is very close to the tip of the nozzle. The pinch off time is constant which means that the drop formation occurs at regular time interval. Also the size of the drop does not change and the shape is well defined and spherical.

In this study, the outlet of tube was wet so that for low flow rates, the liquid reaches the edges of the nozzle. Consequently, the diameter of the exiting fluid is same as the outer diameter of the tube. The tip of the liquid at the nozzle has a nearly spherical shape because of

the surface tension force which tends to reduce the surface area. The surface tension force is due to the unbalanced molecular forces on the surface of the liquid. It is a cohesion force that occurs between molecules of same type. With the fluid inflow, the volume of the nearly formed drop increases and its form changes from spherical to pear-like shape. The diameter of the drop increases and is greater than the exterior diameter of the nozzle (Figure 2.2(j)). Gravity tends to pull the drop down and elongating it axially as the inertial force pushes it away from the nozzle. For a while, the inertial, surface tension and gravitational forces are in equilibrium and the drop continues to grow while still attached to the tube. When the volume of the drop reaches a certain value, equilibrium cannot be maintained and the gravitational and inertial forces take over, creating a downward acceleration. Due to the surface tension, a portion of the liquid mass has a greater diameter and after the loss of equilibrium, the region with the smaller cross section becomes more vulnerable. The bottom part of the fluid starts moving down and since it has a greater weight, its pull on the middle section increases the pressure. The diameter of the middle region gets thinner as the velocity increase (Figure 4.4). This phase of the drop formation is called necking. The width of the region right above the drop keeps decreasing until it becomes a long and thin ligament. Once the necking happens, three distinctive liquid parts can be noticed, with the first one being the portion of mass still attached to the nozzle, the second being a fluid ligament and the last one, a nearly formed drop. The pressure in the neck rises and is greater than that in the other parts. Figures 4.5 shows the fact that there is the maximum pressure at the base of the neck where the radius has the lowest value. Since the radius is inversely proportional to the curvature, the smaller the radius, the greater the curvature. The Young-Laplace equation (Equation 3.17) establishes the relation between the pressure at the interface and the local curvature and predicts that a large curvature would generate a pressure peak.

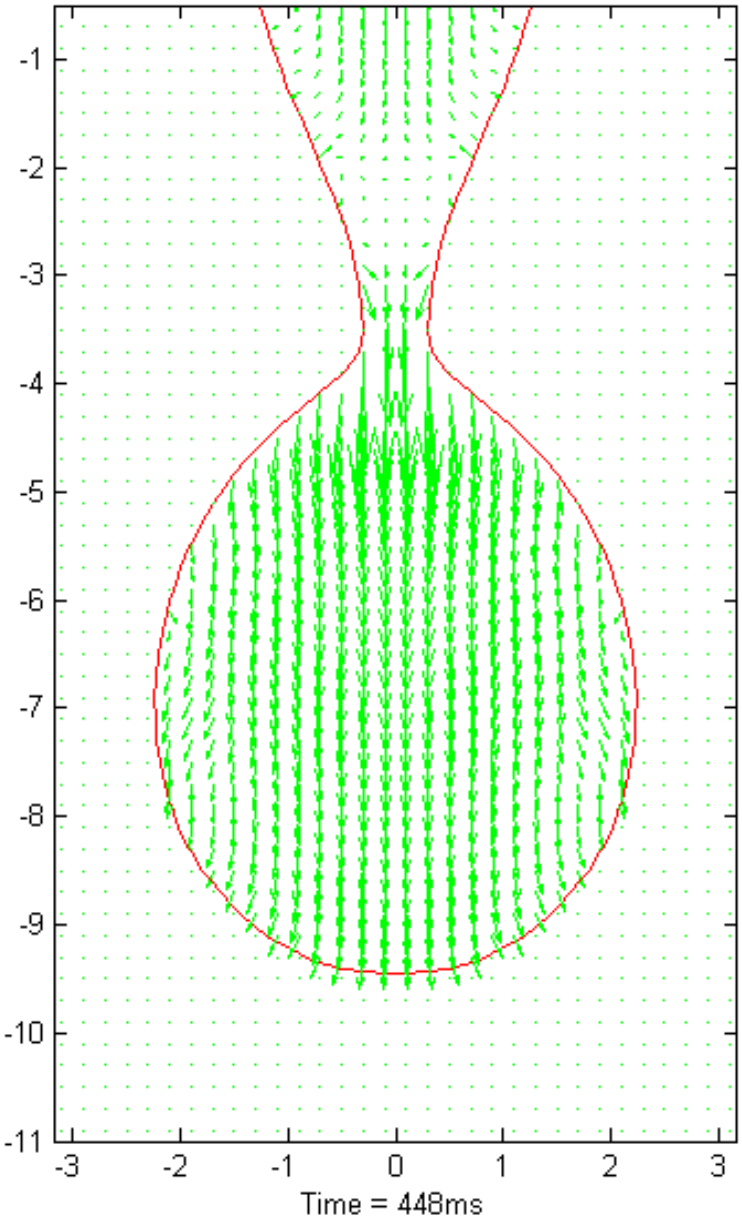

Figure 4.4 Velocity profile during necking

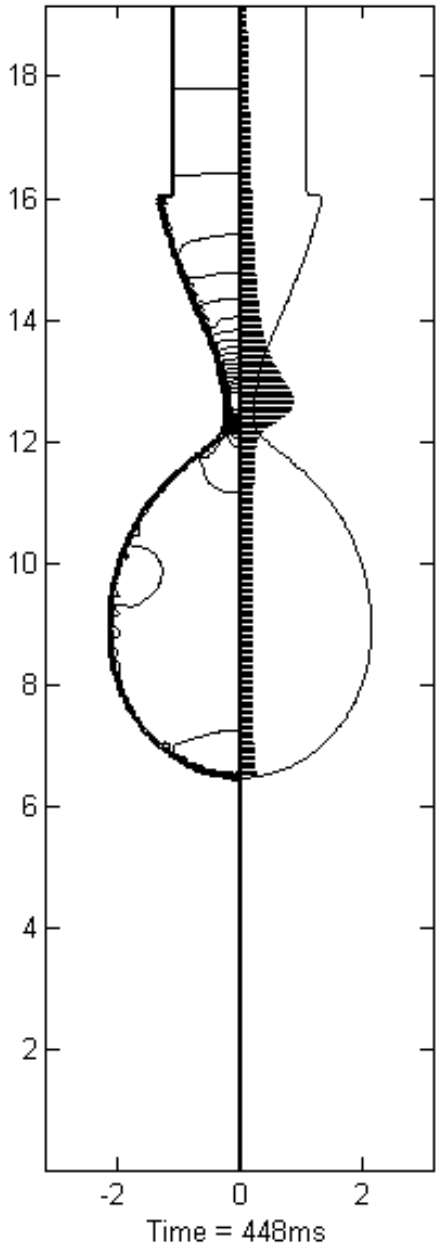

Figure 4.5 Pressure profile during necking

The liquid continues to flow from the tube; however once necking is initiated, the fluid does not come into the thin ligament because the detachment of the drop occurs shortly after the necking has started. The time for break up is very short and in the present cases studied, it was in the order of milliseconds. Not only there is no addition of fluid in the necking section, the high pressure gradient favors a squeeze of liquid out of the liquid bridge. The velocity and the pressure have the highest magnitude at the base of the neck; the radius at this precise point becomes very small (Figures 4.6 and 4.7) and eventually breaks up, disconnecting the drop. The newly formed drop is called primary drop and has a flat surface at the place where it used to be attached to the neck (Figure 4.8). The flattened side of the drop is due to the fact that after the break up, the inertial forces are dominant and the velocity pushes down on the top part. Moment later, under the action of the surface tension, the shape of the drop is restored to spherical form and it falls due to gravity. After the detachment of the main drop, the liquid bridge recoils because of the action of the surface tension force which as always, aims to minimize the surface area; therefore the tip of the ligament becomes rounded and moves up as shown on Figure 4.8. In fact, after the pinch off, there is an unbalance of forces which results in an upward acceleration. Depending on certain conditions, the liquid thread can disengage from the portion of the fluid connected to the tube and form another droplet called satellite drop. There are two cases in the periodic dripping regime: one is the formation of drop with satellite and the other is the formation of drop without satellites.

The main parameter for the formation of satellite is the Weber number which measures the relative importance of the inertia to surface tension forces [2]. The Weber number is used instead of the velocity because the concept of low or high velocity is relative. Depending on the nozzle diameter, a certain velocity magnitude may be considered high or low. For example, in Table 4.2, the velocity value of 0.08m/s is low for a tube of inner diameter D=2.10mm and there is the formation of satellite droplets; however the same velocity is considered pretty high for a tube of inner diameter D= 4.1mm and there is not satellite formation.

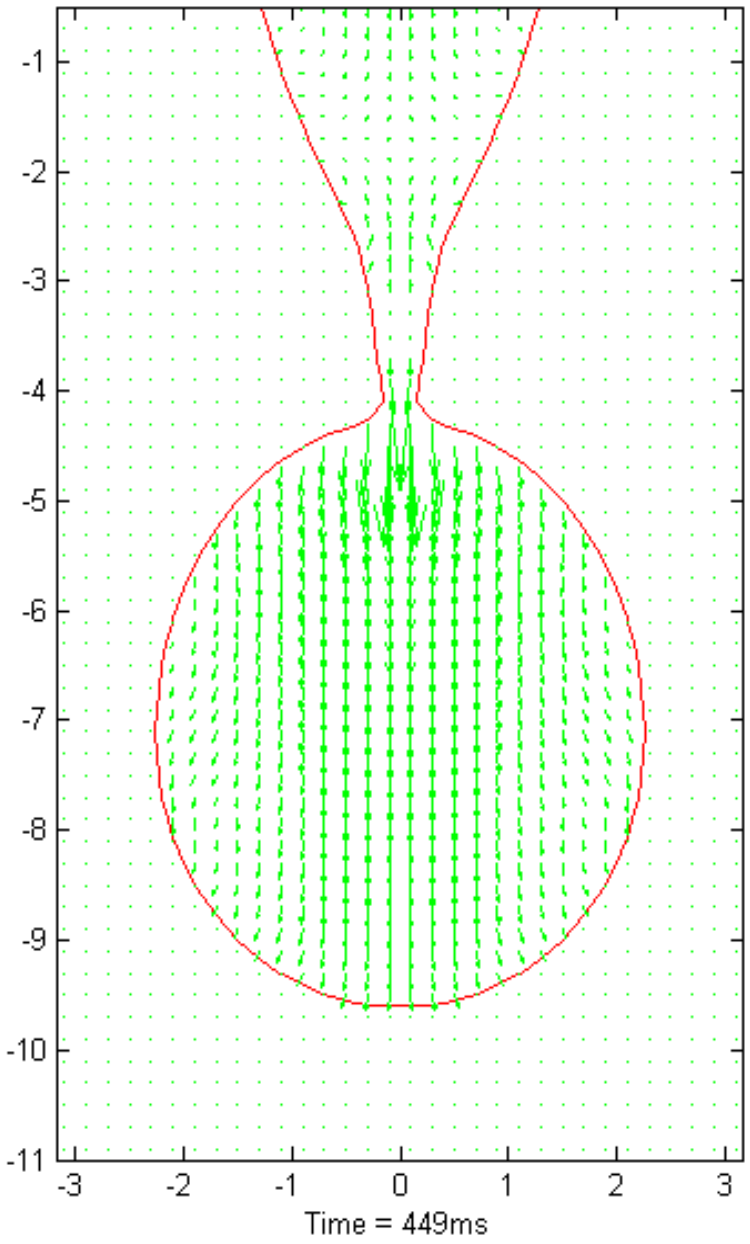

Figure 4.6 Velocity profile just before the pinch off

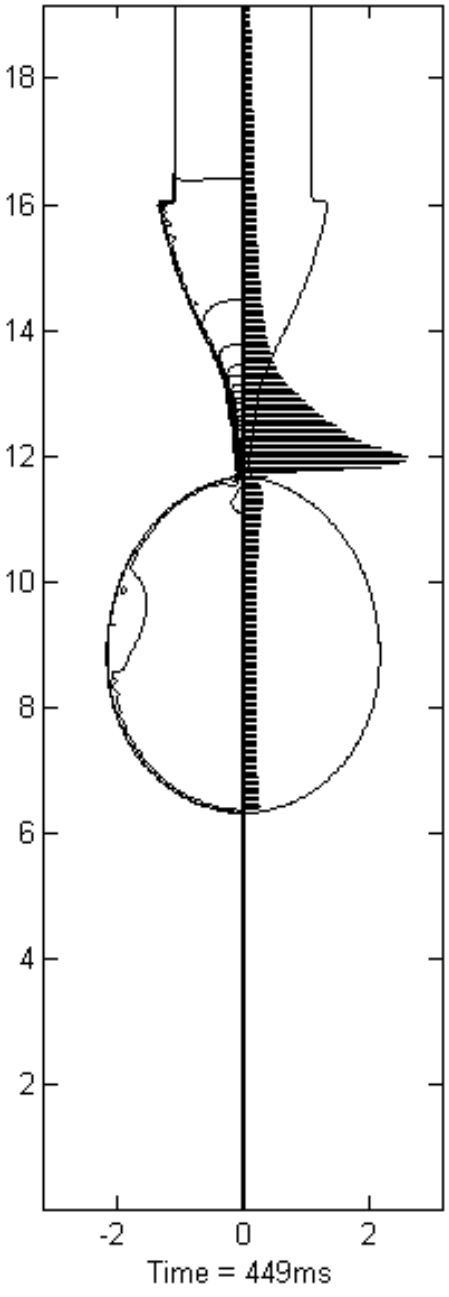

Figure 4.7 Pressure profile just before the pinch off

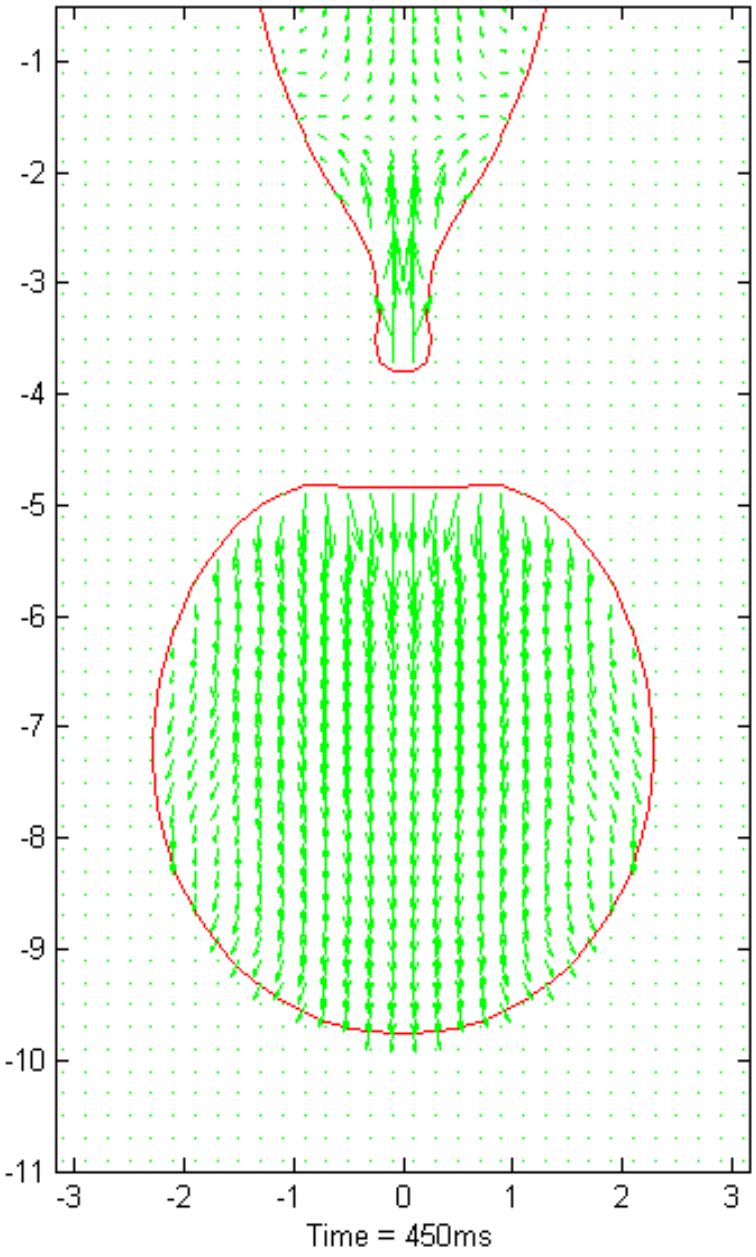

Figure 4.8 Velocity profile just after the pinch off

There is formation of satellite drops after the detachment of the main drop during the periodic dripping regime for small Weber numbers. Sometimes, the liquid thread becomes very thin during the necking and because the pinch off generates some perturbations on its surface, it could become unstable and break up into satellite drops (Figures 4.9 and 4.10). Unlike the detachment of the primary drop which was due to the loss of equilibrium, the breakup of the ligament from the main system is due to disturbances born from the first break up. Henderson and co-workers [8] studied the evolution of the liquid ligament and showed that break up occurs under the action of instability.

Depending on the size of the satellite, it may move up or down. As stated previously, after the detachment of the primary drop, the ligament, precursor to satellite drops, moves up due to the effect of the surface tension. After its transformation is satellite drop, it falls under the influence of the gravitational and surface tension forces [6]. The volume of the drop will determine which force will have the greater effect. If the satellite is small enough, the surface tension wins and the droplet keeps moving up merging with the part of the liquid connected to the tube. This is shown in Figure 4.9, where the satellite coalesces with the upper portion of the system. When the satellite has a greater volume, the gravity force takes over and there is a movement downward [6]. This is shown in Figure 4.10, where after its formation, the satellite drop falls down, following the main drop.

In the periodic dripping regime, when the Weber number is increased, there is no formation of satellite drops. In fact, when the velocity is higher, there is more liquid flow along the whole ligament. The tip of the ligament is thicker and there is no break up due to instabilities. As shown on Figure 4.11, the liquid thread does not break up in satellites even though it is longer than that of the case of a lower Weber number.

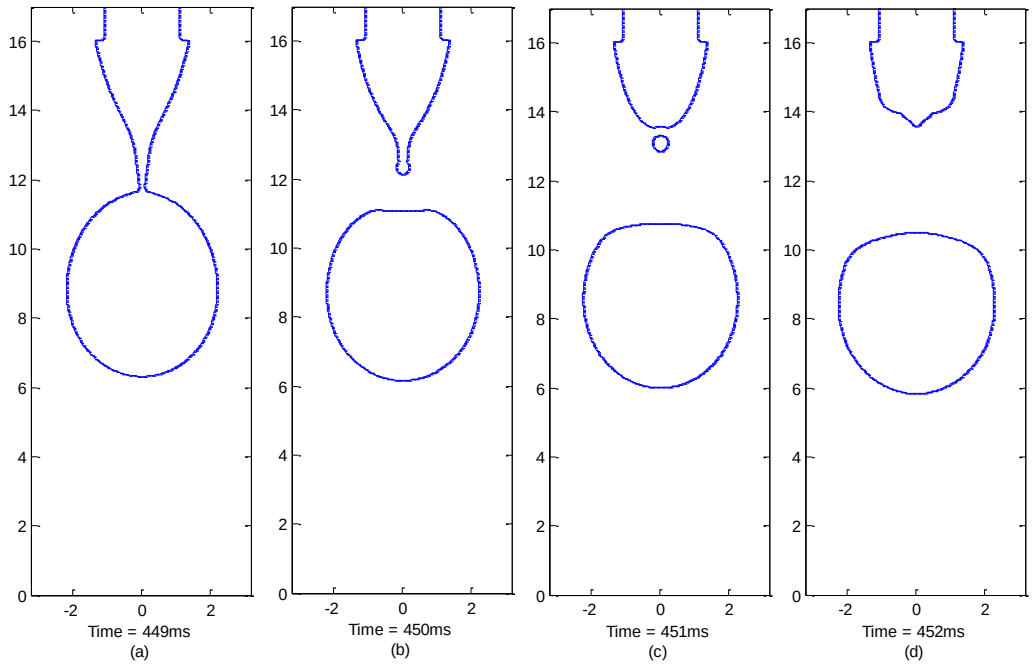

Figure 4.9 Formation of satellite drop after the detachment of the main drop, for a capillary tube of inner diameter D=2.1mm and outer diameter Do=2.7mm for a liquid velocity of 0.08m/s.

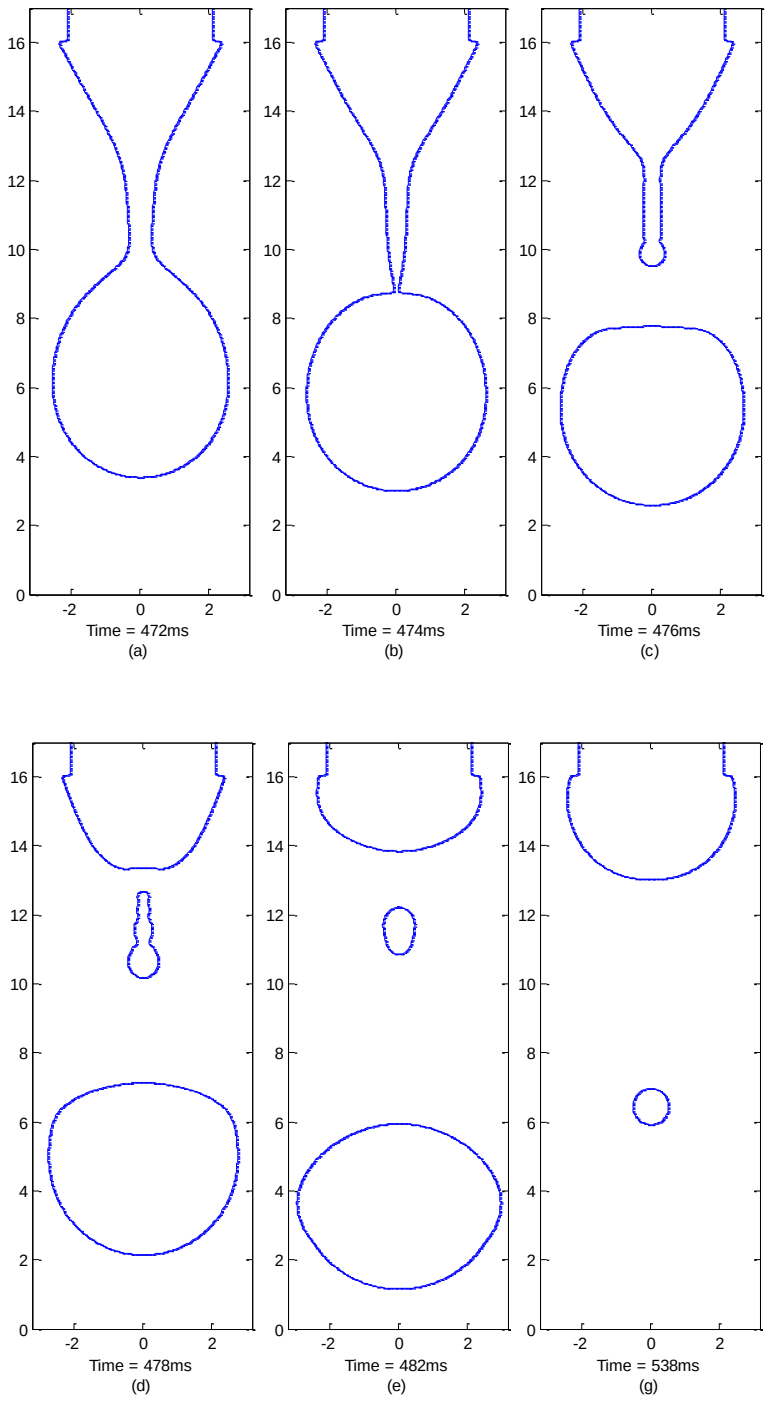

Figure 4.10 Formation of satellite drop after the detachment of the main drop for a capillary tube of inner diameter D=4.1mm and outer diameter Do=4.7mm for a liquid velocity of 0.02m/s.

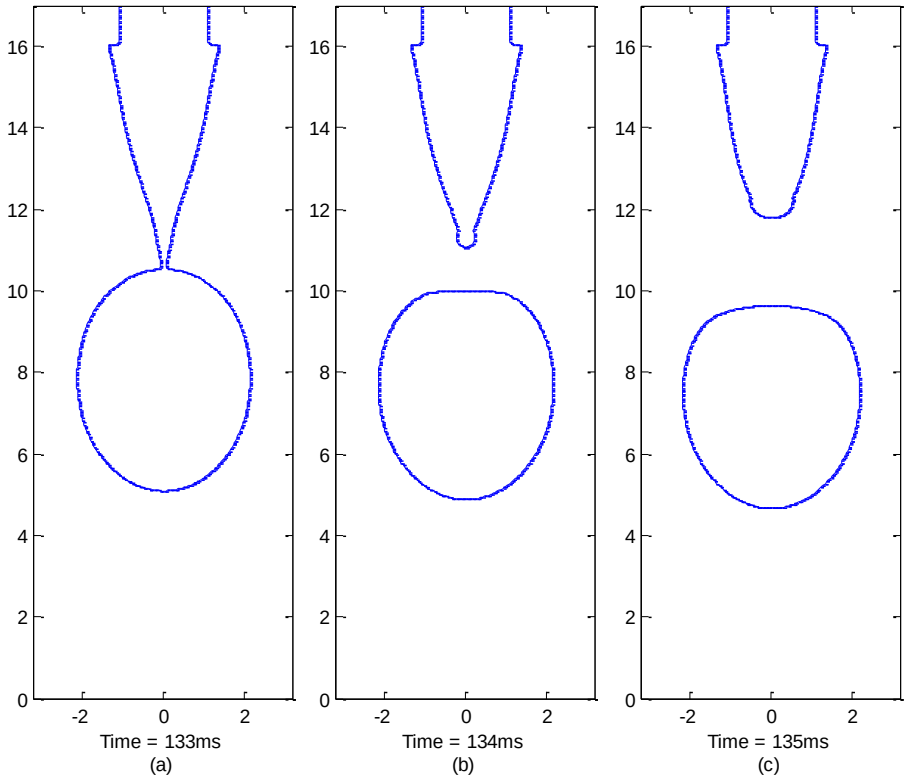

Figure 4.11 The breakup of the main drop with no satellite formation for a capillary tube of inner diameter of D=2.1mm and outer diameter Do=2.7mm for a liquid velocity of 0.15m/s.

4.7.2 Dripping Faucet

This is the second regime and it is characterized by a slightly higher velocity or Weber number. The detachment point is lower than in the first regime, but it does not move away from the nozzle. One main feature of this regime is the formation of a big drop followed by smaller ones. The dripping faucet regime is sometimes called the chaotic dripping regime because it has multiple periodic bifurcations which are difficult to predict. As reported in Table 4.2, different patterns have been noticed in the present study. In Figure 4.12, there is a dripping faucet mode with three different periods of drop formation, where in Figure 4.13, the dripping faucet regime has only two periods. In this regime, successive drops have different sizes but depending on the number of periods, there is a repetition of the drop sizes. As shown in Figure 4.12, the first and fourth drops are the same. Also Figure 4.13 shows another phase of dripping faucet where there is the alternative formation of a big drop and a much small one.

Even though the detachment pattern in the dripping faucet cannot be generalized to all cases of the formation of drop from a capillary tube, it is known that the physical properties of the fluid such as surface tension, viscosity and density shape the dripping faucet regime and determine its condition of existence [10]. Since the process of drop formation does not really depend on the magnitude of those properties but rather on their relative importance, dimensionless numbers are widely used. In the study by Subramani et al. [10], when the Ohnesorge number, Oh (Equation 4.2), a measure of the importance of viscous to surface tension force was increased while the other variables were held constant, the velocity span over which the dripping faucet occurred, was drastically reduced. The Ohnesorge number, Oh, is defined as:

$$Oh = \frac{\mu}{\sqrt{\rho \sigma D}} \qquad 4.2$$

where ρ is the fluid density, D is the inner diameter of the tube, μ is the fluid viscosity, and σ is the fluid surface tension.

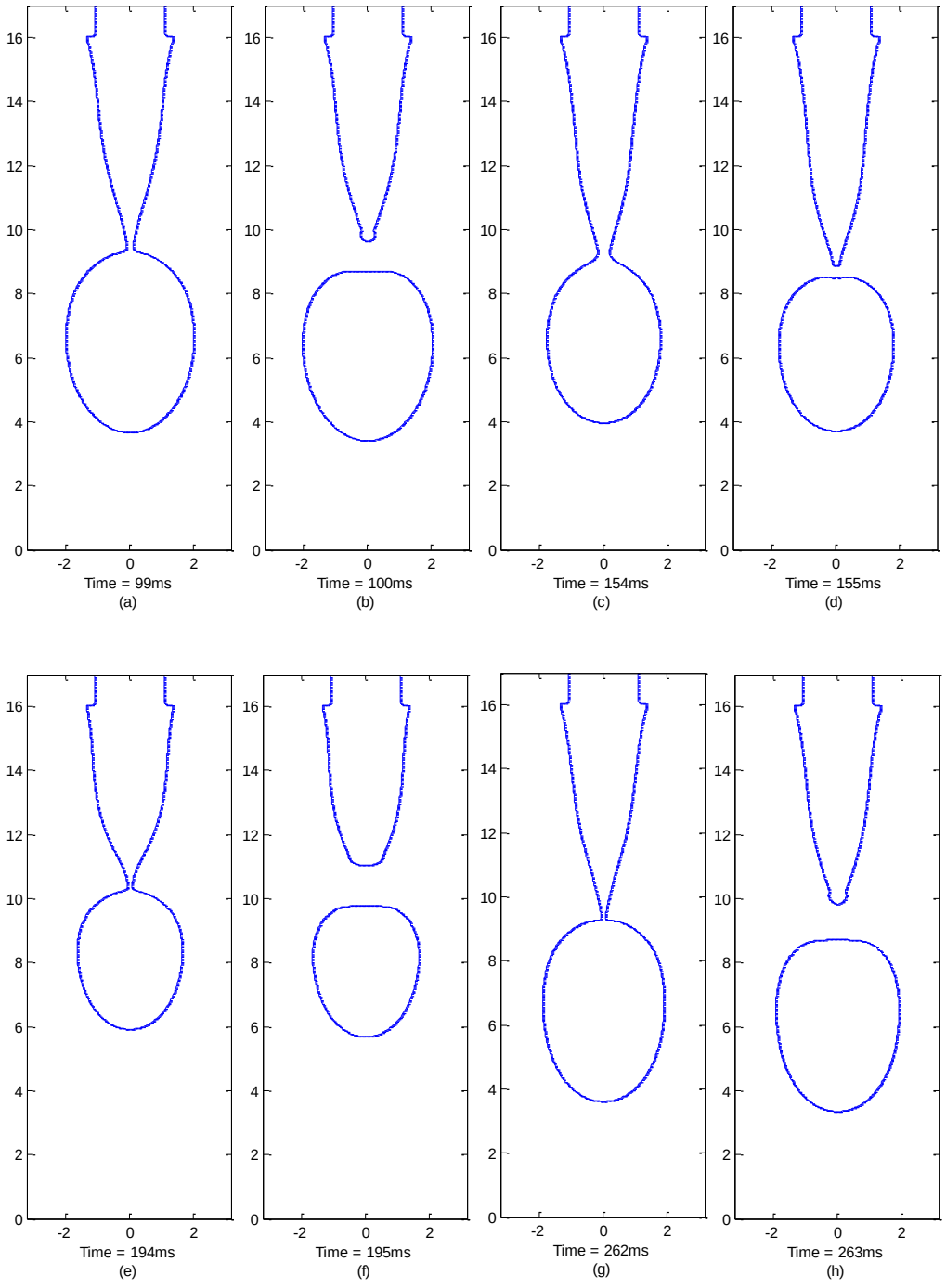

Figure 4.12 Dripping faucet regime with triple periodic drop detachment for a liquid velocity of 0.20m/s: (a)-(b) first drop, (c)-(d) second drop, (e)-(f) third drop, (g)-(h) fourth drop

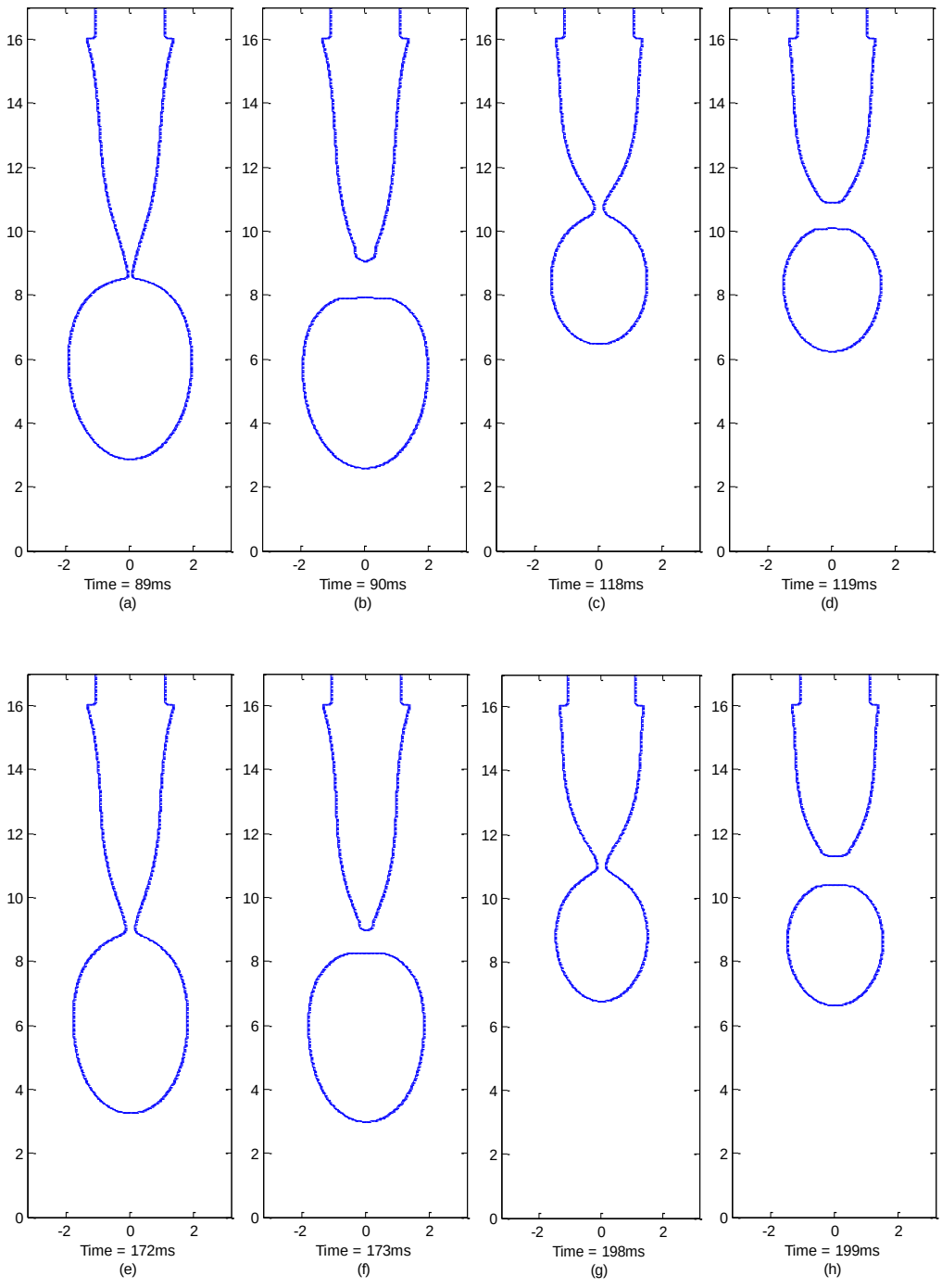

Figure 4.13 Dripping faucet regime with double periodic drop detachment for a liquid velocity of 0.22m/s: (a)-(b) first drop, (c)-(d) second drop, (e)-(f) third drop, (g)-(h) fourth drop

For some cases where the viscosity was very high and dominant, the dynamics of drop formation went directly from periodic dripping to jetting, without exhibiting the dripping faucet regime. Another fact that came to attention is the role of the Bond number, B_0. The Bond number is the ratio of the gravitational to surface tension forces and is defined as:

$$B_0 = \frac{\rho g D^2}{\sigma} \qquad 4.3$$

where g is the gravitational acceleration.

On the complex dripping regime, for low value of B_o (B_o is 0.3 in [10]), there was only one type of dripping faucet with a double period. By keeping the nozzle dimensions, surface tension, viscosity constant while changing the Weber number, as was done in this study, the dripping faucet regime exhibits different characteristics and different periods; however for low B_o number, the dripping faucet has only two periods, even when the Weber number changes [10].

As seen on Figure 2.3, in the dripping faucet regime, the length of the fluid before necking is quite long comparing to that of the periodic dripping because of the velocity increase. The mechanism of formation of the primary drop in the dripping faucet regime is the same as that of the periodic dripping where the drop is formed after the loss of equilibrium between the different forces. However, in the case of the second drop, the different oscillations born from the first pinch off participate in the mechanism of formation. It could be noticed that in both dripping faucet and periodic dripping, there are oscillations on the liquid ligament after the breakup of the first drop; however, in the dripping faucet, the liquid ligament is longer (Figure 2.1) and is more affected by the growth of the oscillations. After the detachment of the primary drop, there is an unbalance of forces where the surface tension is dominant. The force unbalance creates on the surface of the remaining liquid filament, some oscillations which grow in magnitude and initiate the breakup of a second drop. The oscillations enhance the action of the gravitational and inertial forces and provoke an early pinch off; therefore the second drop formed has slightly less volume than the primary drop. Had the growth of the perturbations not occurred, the size of the

second drop would have been same as the first one. In the absence of perturbations, the surface tension has more influence and bigger drops are created. This is confirmed in an experimental study by Subramani et al. [10] which showed that there was not a dripping faucet regime for highly viscous fluid. The role of viscosity is to damp the oscillations and halt their growth; thus, the higher the viscosity, the less effect the perturbations will have on the dynamics of drop formation and the more time the surface tension will have to influence the process. Also it was noticed that when the viscosity increased, the number of periods in the dripping faucet regime was reduced.

As stated previously, there were chaotic bifurcations in the dripping faucet regime with the formation of different drop sizes when the velocity changes. Figures 4.12 shows a case where the inner and outer diameters are respectively 2.1mm and is 2.7mm; when the velocity is 0.20m/s there are three different periods of drop formation and by increasing the velocity to 0.22m/s, the number of periods becomes two. The dripping faucet regime for the others cases studied (Table 4.2) showed the same trend: multiple periodic detachments. In some of the cases studied in the present paper, the viscosity was changed and it was observed that the dripping faucet disappears when the viscosity reaches a certain value. This founding is in agreement with other researches [10] where it was demonstrated that for very high viscosity, there was no dripping faucet regime. The different drop sizes observed during transition from dripping to jetting is due to the action of the perturbations. In the absence of those perturbations, the dynamics of drop formation is same as in the periodic regime and is only due to the loss of equilibrium between the different forces.

4.7.3 Jetting

The third regime in which the fluid has the highest velocity is the jetting. In this regime, the detachment point of the drops is lower than that of the two other regimes. When the jetting velocity is close to the second limit (limit between dripping faucet and jetting), the drops are first

formed near the nozzle tip, then the detachment point moves away until the drops are formed from the ends of a long liquid column. It was also noticed from Figure 4.14 that the drops have different sizes. For very high velocity, the pinch off position of the first drops is far from the nozzle tip, at a distance of about 10Do [2].

In this paper, the jetting regime with velocity close to the second limit is studied and only the formation of the first drops was observed because of the length of the computational domain (Figure 4.14). The simulation was stopped when the length of the liquid column was greater than the length of the domain. The formation of drops from a long liquid column was not of interest in the present study but it has been the subject of other researches [9, 12, 21].

The mechanism of drop formation in the jetting regime is very complex and involves many parameters. In general, the drops are generated from the combined action of the different forces and instabilities. Depending on the pinch off position of the drop, some parameters are dominant comparing to the others. When the drops are formed near the nozzle tip, the gravitational, inertial and surface tension forces play an important role in the break up mechanism comparing to instabilities. In fact, for a jetting velocity close to the second limit, the drop formation is quite similar to that of the dripping faucet. The drops are formed by the action of the forces and the oscillations born from the break-up of previous drops. The oscillations grow in magnitude and help the gravitational and inertial forces against the surface tension to provoke a pinch off. The mechanism of drop formation changes when the inertial force becomes dominant and the drops are formed far from the nozzle tip. In fact, the velocity pushes the liquid particles further down, creating a much longer ligament. Because the liquid ligament is quite long, it is susceptible to instabilities and breaks up in drops due to the growth of the perturbations. For a long liquid column, the growth of instabilities becomes dominant comparing to the different forces. The type of instability that affects the liquid column is called the Plateau-Rayleigh instability [9, 12].

The Plateau-Rayleigh instability is due to the growth of perturbations present on the surface of the liquid column. Those perturbations have a wavy form and grow larger in time. They affect the shape of the liquid column and reduce its radius until it breaks into droplets. In fact, as the disturbance grows, there is deformation of the column and a change in the pressure distribution. The pressure in the column is highest at the sections which have the smallest radius (Equation 3.17). Those sections are the area where there will be pinch off.

At a given instant, there are many growing perturbations with different growth rate. The wave with the maximum growth rate is called the fastest growing mode. This particular wave has the greatest amplitude and initiates drop formation. In order to determine the fastest growing wave, the findings of Plateau [12] and Rayleigh [9] are used. From those findings, the dispersion equation was derived [21]. This equation demonstrated that when the length of the liquid column is greater than the wavelength of the fastest growing wave, there is a possibility that the column will decompose into droplets.

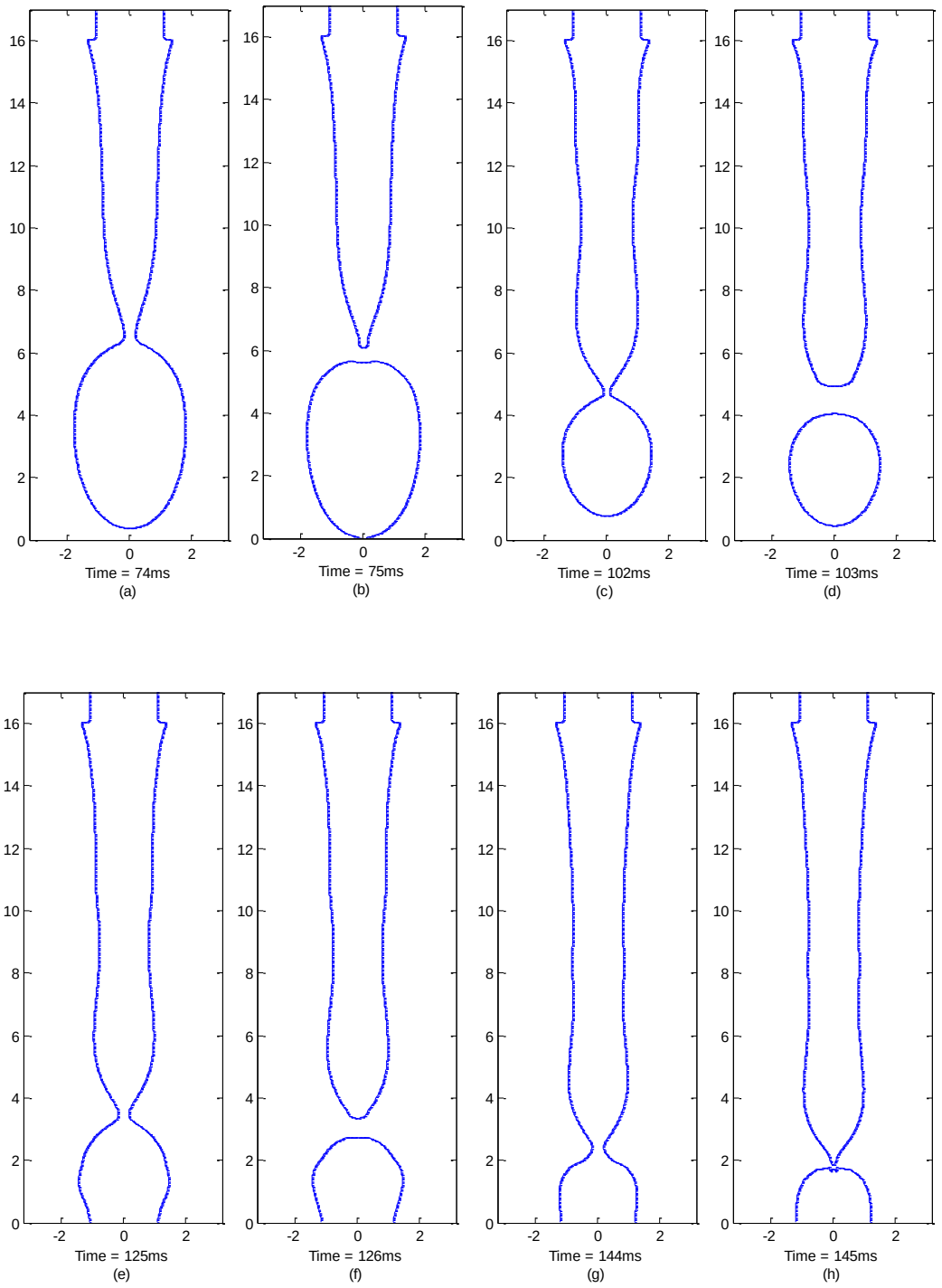

Figure 4.14 Jetting regime with different drop detachments for a liquid velocity of 0.27m/s: (a)-(b) first drop, (c)-(d) second drop, (e)-(f) third drop, (g)-(h) fourth drop

CHAPTER 5

CONCLUSIONS AND FUTURE WORK

The mechanism of drop formation from a capillary tube has been studied using numerical simulations. The free surfaces of the fluid are computed with the Coupled Level Set Volume of Fluid (CLSVOF) method and are reconstructed with the Piecewise Linear Interface Calculation (PLIC) scheme. The Continuum Surface Force (CSF) model is used to estimate surface tension force at the interface. The numerical simulation has many advantages since it permits to observe in great detail the mechanism of drop formation in the different regimes.

In order to observe the different regimes of drop formation, the velocity of the incoming fluid is gradually increased. There are three main regimes of drop formation from a capillary tube. The first regime which has the lowest flow rate and where the drops formed have the same size is called the periodic dripping. The drops are generated after the loss of equilibrium between the forces. When the flow rate is slightly increased, the periodic dripping gives way to the dripping faucet which is characterized by multiple periodic bifurcations. In this regime, successive drops have different sizes but depending on the number of periods, there is a repetition of the drop sizes. The drops are formed due to the combined influence of the different forces and the oscillations born from the detachments of precedent drops. In the third regime which is the jetting mode, the detachment point of the drop move away from the tube exit and the drops are formed from the end of a long liquid column. The mechanism of drop formation depends on the detachment position. When the drops are formed close to the nozzle exit, the different forces acting on the fluid are dominant comparing to the disturbances. When the detachment position is far from the nozzle tip, the drops are mostly formed by the growth of perturbations or the action of the Plateau-Rayleigh instability.

The simulations were run for multiple tube dimensions, and velocity limits between the regimes were obtained. There were two velocity limits with the first one being the limit between the periodic dripping and the dripping faucet and the second limit being the one between the dripping faucet and the jetting. Those velocity limits were function of the outer diameter of the tube and could be used as a way to predict the regime of drop formation. The action of the viscosity on the two limits was studied. It was found that increasing the viscosity only affects the first limit and reduces the velocity range over which the dripping faucet exists. The numerical results were compared to available experimental data and a good agreement was found.

For future work, the Pressure Boundary Method (PBM) could be incorporated to the computer code to replace the CSF model in order to suppress the spurious currents and interface instabilities. Moreover the jetting regime with higher velocity could be fully investigated by increasing the length of the computational domain and studying the effect of the Plateau-Rayleigh instability.

APPENDIX A

CODE EXECUTION

The program code used in this study was written in FORTRAN as the programming language for the UNIX environment [17]. In setting up a problem for a computation, the user must furnish the problem geometry, initial conditions, fluid properties, numerical parameters, the I/O (input/output), the surface reconstruction method, and the scheme either the VOF or the CLSVOF. The information is fed to the compiled executable file with the *input* file in which the variables are grouped into format-free namelists. Several modifications, such as the boundary conditions, are done to the source code. A sample *input* file and the details of the modifications are given in Appendix B. Further information on setting up the problem can be found in [1] and [16].

The calculations are performed on the High Performance Computing (HPC) environment of The University of Texas at Arlington. The system operates with Compaq ES40 Alpha servers with quad 833MHz 64-bit EV68 and Compaq DS20E Alpha servers with dual 667MHz 64-bit EV67 processors. Four files are required to be placed in a same directory for running a simulation: the *input* file, the *file_nam.dat* file which contains the number and names of output data, the *bjob* file which contains the load sharing facility (LSF) instructions, and the compiled executable, *ripple*. The program periodically saves a data file at that time instant according to the outputting frequency specified in the *input* file. The number of files to be generated is followed by the *file_nam.dat* file. If the program generates more than the numbers specified in the *file_nam.dat* file, the last file is overwritten until the program finishes the computation. Each output data file contains the solutions in a specified format as follows:

1. The first and last real cells in the r- and z-direction
2. Location of the left side of each computational cell in the r-direction of the lower side of each computational cell in the z-direction
3. Data : the velocity in the r-direction, the velocity in the z-direction, the volume fractions (VOF function value), the level set (LS) function value, the enthalpy, and the pressure.

A sample output data file is given in Appendix B.

In the present study, the post processing of the data obtained from the simulation was done with the help of the software MATLAB, which loads the data file and generates various plots to analyze the results.

APPENDIX B

SAMPLE INPUT AND OUTPUT

B.1 Sample INPUT

Several modifications were done to the program code to simulate pendant drop formation [17] for the present study. The files which were modified are: *bc.F*, *newcyc.F*, *comdk1.h*, *rinput.F*, and *tapin.F*. Boundary conditions along with nonslip, no-penetration, and inlet velocity profile are specified by the subroutine *bc.F*. Parameters of corresponding conditions are given in the namelist GRAPHICS in the input file as follows:

iout(21): the number of cells from $r = 0$ to $r = R_i$,

iout(22): the number of cells from $r = 0$ to $r = R$,

iout(24): the flag for the inlet velocity profile: 1 for a parabolic profile;

otherwise, a uniform profile,

with R_i, the inner radius of the nozzle and R_i the outer radius of the nozzle.

Since the breakup occurs in a very short period, the frequency of outputting data files was modified to be variable for a specific period with an arbitrary frequency. By generating data files in the vicinity of pinch-off in time, the computational resources can be saved in terms of storage and time. The following three parameters were added to adjust the output frequency: *ppltdt*, *pstart*, and *pperiod*. These parameters are specified in the namelist NUMPARAM in the *input* file. The explanation of the new parameters is given below.

PPLTDT: the frequency of generating data files when (*pstart*) $\leq t \leq$ (*pstart* + *pperiod*)

PSTART: the time period to keep the new outputting frequency, *ppltdt.* The frequency of generating data files is switched back to the original period, *pltdt*, after *pperiod*.

PPERIOD: the duration to switch *pltdt* to *ppltdt*

A sample *input* file is shown below. All the other parameters are taken over from a previous version of the code. Further details of them are available in [1], [16] and [22].

```
run032  c029c 050223 CLSVOF [mm,ms,mg,K]
$numparam
alpha=2.0,
autot=1.0,
conserve=.false.,
delt=1.0e-5,
dtmax=4.14e-3,
twfin=200000.0,
con = 0.3,
fcvlim=0.5,
idiv=1,
dmpdt=300000000.0,
prtdt=100000000.0,
pltdt= 1.0,
ppltdt= 1.0,
pperiod= 1.0,
pstart= 2000.0,
sym=.true.,
kt =6,
kb =6,
kl =1,
kr =3,
gfnctn=.true.,
$end
$fldparam
gy= -9.81e-3,
icyl=1,
canglel=90, cangler=90, canglet=90, cangleb=90,
isurf10=1,
psat=0.0,
xnu=1.005e-3,
rhof=1.0,
sigma=7.27e-2,
vi= -0.0,
vinf(2)= -0.06549,
vinf(1)= -0.45,
$end
$mesh
nkx=1,
xl = 0.0, 3.2,
xc= 1.6,
nxl = 16,
nxr = 16,
dxmn= 0.1,
nky=1,
yl= 0.0, 19.20,
yc= 9.60,
nyl= 96,
nyr= 96,
dymn= 0.1,
$end
$obstcl
```

```
nobs=3,
ob1(1)=-1.0, oc1(1)= 16.0, ioh(1)=1,
oa1(2)= 1.0, oc1(2)= -1.0, ioh(2)=0,
oa1(3)= -1.0, oc1(3)= 1.6, ioh(3)=0,
$end
$freesurf
nfrsrf=6,iequib=0,
fc1(1)= -1.0, ifh(1)=1,
fb1(2)= -1.0,fc1(2)= 16.0,ifh(2)=0,
fa1(3)= -1.0,fc1(3)= 1.0,ifh(3)=1,
fb1(4)= 1.0, fc1(4)= -16.0, ifh(4)=0,
fb1(5)= 1.0, fc1(5)= -15.9, ifh(5)=1,
fa1(6)= -1.0, fc1(6)= 1.6, ifh(6)=1,
$end
$graphics
plots=.true., dump=.false.,
iout = 0, 1, 0, 0, 0, 0, 0, 0, 0, 0, 0, 0, 0,
0, 0, 0, 0, 0, 0, 0, 10, 16, 0, 1, 0, 0,
0, 0, 0, 0, 0, 0, 0, 1, 0, 1, 1, 0, 1,
iysymplt=1,
$end
$heateq
heat = .false.,
ischeme = 3,
tid = 525.0,
tip = 300.0,
tia = 100.0,
cpp = 227.0,
cpd = 227.0,
cpa = 50.0,
tkp = 432.2,
tkd = 67.0,
lhpc = 58900.0,
hmr = 5.0,
tl = 510.0,
ts = 505.0,
teps = 1.0e-8,
$end
$coupled
lsvof=.true.,
ls = .false.,
$end
```

B.2 Sample OUTPUT

The data files contains the solutions of the governing equations are named according to the *file_nam.dat* file. A sample output file and its explanations [17] are given below.

```
0.00000E+000  <----- time
2, 32                    <----- 1st real cell, last real cell in r-direction
2,192                    <----- 1st real cell, last real cell in z-direction
0.00000E+000  <----- location of the left side of each computational
1.00000E-001          cell in the r-direction
2.00000E-001
3.00000E-001
4.00000E-001
5.00000E-001
6.00000E-001
.
.
.
0.00000E+000   <----- location of the left side of each computational
1.00000E-001            cell in the z-direction
2.00000E-001
3.00000E-001
4.00000E-001
5.00000E-001
6.00000E-001
7.00000E-001
8.00000E-001
9.00000E-001
1.00000E+000
.
.
.
0.00000E+0,-4.50000E-1, 0.00000E+0, 1.00000E+6, 0.00000E+0, 0.00000E+0
0.00000E+0,-4.50000E-1, 0.00000E+0, 1.00000E+6, 0.00000E+0, 0.00000E+0
0.00000E+0,-4.50000E-1, 0.00000E+0, 1.00000E+6, 0.00000E+0, 0.00000E+0
0.00000E+0,-4.50000E-1, 0.00000E+0, 1.00000E+6, 0.00000E+0, 0.00000E+0
0.00000E+0,-4.50000E-1, 0.00000E+0, 1.00000E+6, 0.00000E+0, 0.00000E+0
. (comp. 1),    (comp.2),    (comp. 3),    (comp. 4),    (comp.5),    (comp.6)
.
```

In the above six-column matrix, components from comp.1 to comp.6 show the following solutions:

comp.1: velocity component in r-direction

comp.2: velocity component in z-direction

comp.3: VOF function value

comp.4: LS function value

comp.5: enthalpy

comp.6:pressure.

REFERENCES

[1] Kothe, D. B., Mjolsness, R. C. and Torrey, M. D., “RIPPLE: A Computer Program for Incompressible Flows with Free Surfaces", Tech Report. LA-12007-MS, 1994.

[2] Clanet, C. and Lasheras, J. C., “Transition from dripping to jetting”, *J. Fluid Mech.,* Vol. 383, 1999, pp.383-326.

[3] Tate, T., “On the magnitude of a drop of liquid formed under different circumstances”, *Phil. Mag.*, Vol. 27, 1864, pp.176-180.

[4] Rayleigh, Lord, “Investigations in capillarity: the size of drops. – The liberation of gas from supersaturated solutions. – Colliding jets. – The tension of contaminated water-surfaces. – A curious observation”, *Phil. Mag.,* Vol. 48, 1899, pp.321-337.

[5] Harkins, W. D. and Brown, F. E., “The determination of surface tension (Free surface energy), and the weight of falling drops: the surface tension of water and benzene by the capillary height method”, *J. Am. Chem. Soc.,* Vol. 41, 1919, pp.499-524.

[6] Zhang, X. and Basaran, O. A., “An experimental study of dynamics of drop formation", *Phys. Fluids*, 1995, pp.1184-1203.

[7] Notz, P. K., Chen, A. U. and Basaran, O. A., “Satellite drops: Unexpected dynamics and change of scaling during pinch-off", *Phys. Fluids*, Vol. 13, No.3, 2001, pp.549-552.

[8] Henderson, D., Segur, H., Smolka, L. B. and Wadati, M., “The motion of a falling liquid filament”, *Phys. Fluids,* Vol. 12, No. 3, 2000, pp.550-565.

[9] Rayleigh, Lord, “On the instability of jets”, *Proc. Lond. Math. Soc.*, Vol. 10, 1879, pp. 4-13.

[10] Subramani, J. H., Yeoh, H. K., Xu, Q., Ambravaneswaran, B. and Basaran, O. A., “Simplicity and complexity in a dripping faucet", *Phys. Fluids*, Vol. 18, 2006, pp.1-13.

[11] Savart, E., “Memoire sur la constitution des veines liquides lancees par des orifices circulaires en mince paroi”, Ann. Chim., Vol. 53, 1833, pp.337-386.

[12] Plateau, J., *Statique Experimentale et Theorique des Liquides,* 1873, Gauthier- Villars et C^{ie}.

[13] Ambravaneswaran, B., Wilkes, E. D. and Basaran, O. A., “Drop formation from a capillary tube: Comparison of one-dimensional and two-dimensional analyses and occurrence of satellite drops", *Phys. Fluids*, Vol.14, 2002, pp.2606-2621.

[14] Zhang, X., “Dynamics of growth and breakup of viscous pendant drops into air", *J. Colloid Interface Sci*., Vol. 212, 1999, pp.107-122.

[15] Tong, A. Y. and Wang, Z., “Relaxation dynamics of a free elongated liquid ligament",

Phys. Fluids, Vol. 19, 2007.

[16] Lu, M., “Numerical modeling of multi-phase surface flow", Ph.D. dissertation, Department of Mechanical Engineering, The University of Texas at Arlington, TX,2000.

[17] Kamiya, R., “A Numerical Study of Pendant Drop Formation from a Capillary Tube”, Master’s thesis, Department of Aerospace Engineering, The University of Texas at Arlington, 2005.

[18] Hirt, C. W. and Nichols, B. D., “Volume of fluid (VOF) method for the dynamics of free boundaries", *J. Computational Physics*,vol.39, 1981, pp.201-225.

[19] Brackbill, J. U., Kothe, D. B. and Zemach, C. A., “Continuum Method for Modeling Surface Tension", *J. Computational Physics*, vol. 100, 1992, pp.335-354.

[20] Sussman, M. and Fatemi, E., “An efficient, interface-preserving level set redistancing Algorithm and its application to interfacial incompressible fluid flow", *SIAM J. Sci. Comput.*, vol.20, No.4, 1999, pp.1165-1191.

[21] Santala, M. K. and Glaeser A. M., “Surface-energy-anisotropy-induced orientation effects on Rayleigh instabilities in sapphire”,*Surface Science*, vol. 600, 2006, pp.782-792.

[22] Holt, B. R., “The numerical impact phenomena and solidification of a liquid metal droplet onto a rigid substrate", Ph.D. Dissertation, Department of Mechanical Engineering, The University of Texas at Arlington, TX, 1995.

BIOGRAPHICAL INFORMATION

Allouah Kadjo is from the Ivory Coast in West Africa. She studied mechanical engineering at the University of Texas at Arlington where she graduated in May 2009 with a bachelor degree. She continued her studies at the same institution and received her Master in mechanical engineering in December 2011.